AIMS Mathematics, 10(2): 2891–2929.
DOI: 10.3934/math.2025135
Received: 28 November 2024
Revised: 02 January 2025
Accepted: 08 February 2025
Published: 17 February 2025

http://www.aimspress.com/journal/Math

Research article

Control and optimization mechanism of an electromagnetic transducer model with nonlinear magnetic coupling

Hany Bauomy*

Department of Mathematics, College of Science and Humanities in Alkharj, Prince Sattam Bin Abdulaziz University, Alkharj 11942, Saudi Arabia

* **Correspondence:** Email: hany_samih@yahoo.com.

Abstract: This paper presents a novel nonlinear proportional-derivative cubic velocity feedback (NPDVF) controller for controlling vibrations in systems with both mechanical and electrical components subjected to mixed forces. The proposed controller aims to address the challenges posed by nonlinear bifurcations, unstable motion, and vibrations. The effectiveness of the controller demonstrated through numerical simulations, where it shown to significantly reduce harmful vibrations and stabilize the system under varying operating conditions. To analyze the system, a perturbation technique employed to derive approximate solutions to the system's equations up to the second order at simultaneous resonance case ($\Omega_2 \cong \omega_1, \Omega_4 \cong \omega_2$). A comparative analysis with other control strategies, such as proportional-derivative (PD) control**,** sliding mode control (SMC), and model predictive control (MPC), the superior robustness**,** computational efficiency, and control signal amplitude of the NPDVF controller. Results indicate that the proposed approach not only outperforms traditional methods in terms of energy efficiency and computational cost but also maintains robust performance even in the presence of nonlinearities and parameter uncertainties. The findings support the potential application of the NPDVF controller in real-time vibration control systems.

Keywords: mixed excitations; electromagnetic transducer; perturbation; stability; NPDCVF controllers
Mathematics Subject Classification: 34A34, 37N35,70J99,70K20,74H10

1. Introduction

Generally, electromagnetic transducers are employed to gauge thickness, calculate an object's rotational speed, and detect defects in materials from steel to various other alloys. Managing the nonlinear interaction between vibrating modes is crucial for advancing nano-mechanical or micro-electromechanical devices. Interconnected oscillators serve as primary models aimed at the performance over various technical, chemical, biological, and physical schemes. In nonlinear electromechanical oscillator organizations, the mechanical part functions as a sensor and is magnetically linked to an electrical part, representing a signal of the observed vibration. The space in the permanent magnet facilitates interaction between the mechanical and electrical elements. Chaos management, vacillations, and the stability of a nonlinear electromechanical structure are examined in [1]. Also, an electromechanical gyrostat system that underwent external perturbation for its chaotic behavior, synchronization, and chaotic characteristics (adaptive control, delayed feedback control) observed in [2]. Yamapi and Bowong [3] utilized a sliding mode organizer to manage the electrostatic transducer classification while exploring the dynamic and chaotic behaviors of a self-sustaining electromechanical system both with and without discontinuity. Siewe et al. [4] employed an electromechanical oscillator method to capture the vertical motion of the earth during an earthquake. The application of slight amplitude damping for managing chaos in the system was also investigated. They discovered that the damping coefficient estimation affects both the chaotic and periodic orbits. The interactions and synchronization of two systems studied in [5,6]: a magnetically linked electrical Rayleigh-Duffing oscillator with linear mechanical oscillators, along with an interconnected self-sustaining electromechanical system featuring various functions. They employed the harmonic balance and averaging methods to identify the amplitudes of the oscillatory states. The dynamics, global bifurcations, and chaotic behavior of a self-sustaining nonlinear electromechanical system exhibiting nonlinear dynamics investigated in [7,8]. Moreover, the impact of elevated nonlinearity values on the behavior and synchronization of interconnected electromechanical systems is examined in [9]. Furthermore, the chaotic dynamics and nonlinear oscillations in an electromechanical seismograph system featuring stiffness that varies over time examined in [10]. Also, different types of active controllers are experimented to minimize system oscillations and determined that negative velocity feedback is the most effective active control for the behavior of the system. The influence of noise factors, coupling coefficients, and restraining quantities on the response of an electromechanical seismograph examined in [11].

A time-varying stiffness nonlinear electromechanical seismograph system's behavior, stability, approximate solutions, and dynamic feedback control were all investigated by Amer [12]. He also contrasted the perturbation solution with the numerical solution. Amer et al. [13] examined the performance of a twin-tail aircraft structure with both cubic and quadratic nonlinearities via an active control procedure. Sayed et al. [14–17] examined the non-linear dynamic properties of the rectangular plate within combined excitations. Also, they examined three cases of internal and primary resonances (1:2, 1:1, and 1:1:3) and matched the analytical and numerical solutions of the system. The efficiency of various control procedures in lowering the notable vibrations of a beam was examined by Hamed and Amer [18]. The oscillations and stability of the MEMS gyroscope scheme with distinct parametric forces were investigated in [19]. The frequency response equations for the concurrent resonance situation have been generated using the averaging technique. Dynamical systems motivated by parametric and external influences thoroughly examined in the works of [20,21]. The air

gap of a permanent magnet, which only generates a uniform radial magnetic field, is assumed to reflect the interaction between mechanical and electrical components in most electromechanical system studies. To the best of our knowledge, the assumption of deterministic electromechanical system dynamics has been the sole method used to investigate the effects of this particular magnetic connection. However, when random disturbances are taken into account, these systems can exhibit remarkable characteristics. Similar mechanical systems have previously been shown in the literature to display a variety of behaviours and intricate chaotic dynamics when subjected to noise [22,23]. One kind of instrument that uses electromagnetic transduction to gather vibration energy is an electromechanical seismograph.

Researchers have recently focused on the behavior of electromechanical schemes and their impact on the energy harvesting challenge. The effectiveness of vibration energy harvesting devices influenced by random ambient excitations was analyzed by Martens et al. [24] through the solution of relevant Fokker-Planck equations. Borowiec et al. [25] demonstrated that the noise element of the force influences the system's stability in their investigation of how random excitation affects the performance of an energy harvester. A stochastic averaging method in [26] was introduced to evaluate the mean square electric voltage of a nonlinear energy harvesting system. Li et al. [27] explored a piezoelectric energy harvester featuring tri-stable potential wells persuaded by external magnetic fields. They claimed that the system can be appropriately designed to enhance the frequency bandwidth for a specific deterministic or stochastic input and achieve a high harvesting efficiency at coherence resonance. The multiple scales method (MMS) [28–33] and averaging techniques [34,35] are two perturbation methods commonly employed to analyze the efficiency of parametrically excited models. These methods have proven to remain successful in forecasting the behavior of such systems, especially within the frequency range close to the significant parametric resonance [36]. Traditional MMS are shown to effectively estimate responses in very basic scenarios, such as confined frequency ranges around the central parametric resonance, moderate excitations, and minimal system features [37–43]. Moreover, it has been shown that several control mechanism approaches can reduce the detrimental vibrations produced by different nonlinear systems in [44–52].

This study investigates and manages the nonlinear dynamics and vibration reduction of a model of a nonlinear electromagnetic transducer subjected to parametric and harmonic excitations. The response and stability of the solutions during the most unfavorable resonance cases have analyzed using the perturbation technique [53]. The dynamic response of the sandwiched functionally-graded piezoelectric semiconductor (FGPS) plate with the consideration of the initial electron density is investigated, and the natural frequencies and multi-field coupling are obtained in [54]. Based on the nonlocal piezoelectric semiconductor theory, Fang et al. [55] investigated the transient response of a piezoelectric semiconductor (PS) fiber, and analyzed the bending vibration, electric potential, and concentration of electrons along the nano-fiber with different nonlocal effects. Also, Liu et al. [56] proposed an active disturbance rejection control (ADRC) scheme for the electromagnetic docking of spacecraft in the presence of time-varying delay, fault signals, external disturbances, and elliptical eccentricity. Formerly, Lyu et al. [57] investigated an integrated predictor observer feedback control strategy for the vibration suppression of large-scale spacecraft affected by unbounded input time-delay effects.

The main contributions of this article are summarized as follows:

1) The study introduces a novel control mechanism Nonlinear Proportional-Derivative Velocity Feedback (NPDVF) Controller**,** which integrates nonlinear first- and second-order filters to improve vibration control in systems involving both mechanical and electrical components. This controller is designed to stabilize and suppress vibrations caused by complex nonlinearities and mixed forces within simultaneous resonance case ($\Omega_2 \cong \omega_1, \Omega_4 \cong \omega_2$).
2) The research utilizes the perturbation method to derive approximate solutions for the system equations up to the second order, allowing for a better understanding of the system's behavior under nonlinear conditions. This technique aids in analyzing the stability and response characteristics of the system.
3) A comprehensive mathematical model is presented, which describes the coupled nonlinear ordinary differential equations governing the interaction between the mechanical and electrical components of the system. The model includes cubic and quadratic nonlinearities, which represent the complex behaviors observed in real-world systems.
4) The proposed NPDVF controller is shown to significantly reduce harmful vibrations, mitigate unstable motion, and stabilize nonlinear bifurcations in the system. Numerical simulations demonstrate its ability to handle a variety of excitation frequencies and forcing magnitudes, eliminating self-excited vibrations and improving structural stability.
5) Extensive numerical simulations conducted using MAPLE and MATLAB validate the performance of the controller. The simulations confirm that the NPDVF controller effectively stabilizes the system under mixed force conditions, and the results are consistent with the perturbation analysis, providing strong support for the controller's effectiveness.
6) The examination of stability and the impact of various framework coefficients were assessed together theoretically and numerically.
7) The various nonlinear controllers that influence the system are compared through numerical methods. The primary finding from the numerical result indicates that the new controller NPDVF, is most effective in diminishing and eradicating the model's excessive oscillations.

2. Description of the model equations

A seismograph records ground movement during an earthquake. It falls into the category of electromechanical systems known as electromagnetic transducers. The system being examined is the most basic seismograph as it solely captures the vertical component of ground motion and only accommodates low-frequency movements. It, however, exhibits intricate dynamics. This apparatus is illustrated in Figure 1. In the current study, the electrical component of the seismograph includes a linear inductor L, a linear capacitor C, and a linear resistor R, with their voltage and charge conforming to the following equations.

$$U_C = \frac{q}{C_0} \text{ and } U_R = R\dot{q}, \tag{2.1}$$

where q stands the instantaneous electrical charge, $\dot{q}$ remains its time derivative ($\dot{q} = \frac{dq}{d\tau} = i$, where i is the current).

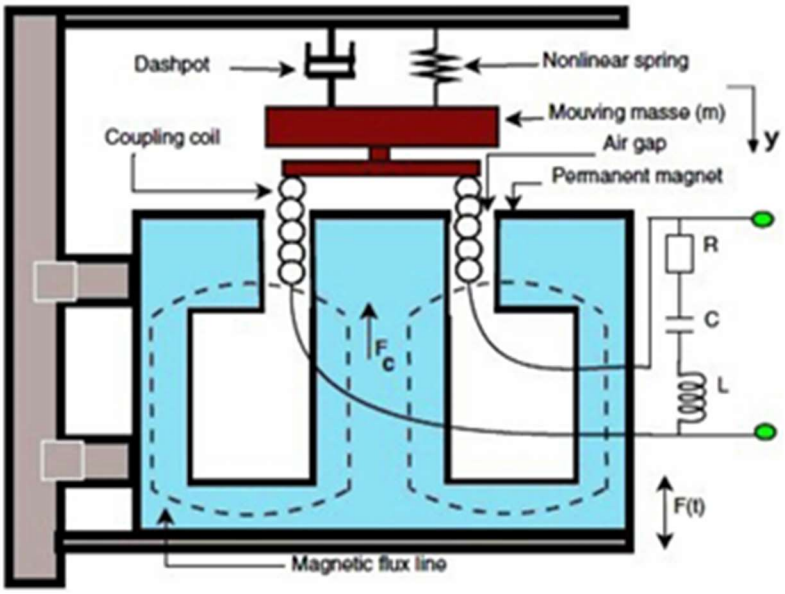

Figure 1. Sketch of an electromechanical seismograph model with associated electric circuit [11].

The mechanical component consists of a suspended mass; its movement is influenced by the intrinsic forces of the mass-spring system and the natural forces affecting the arrangement. Let $F(\tau)$ be the force varying with time that influences the frame because of the ground movement. We assume that damping forces (friction, air resistance, etc.) exist, and the corresponding spring exhibits nonlinear with linear stiffness characterized by k_0; parameters k_1 and k_2 describing the nonlinearity of the stiffness based on its type. The mechanical and electrical components engage via the air-gap of a permanent magnet that generates a radial magnetic field $\vec{B}$. The connection between the magnetic field B and the position of the coil y is considered as:

$$B = B_0\left(1 - \left(\frac{y+y_0}{y_{max}}()^2\right)()\right), \tag{2.2}$$

where B_0 is the greatest intensity that the field B attains occurs, y_0 is the armature's initial position, y remains its oscillation amplitude, and y_{max} represents the maximum amplitude. Subsequently, the movement of the mechanical component must consider the connection between the Laplace force and the current indicated by:

$$F_C = \alpha_0\left(1 - \left(\frac{y+y_0}{y_{max}}()^2\right)(\dot{})\right). \tag{2.3}$$

While in the electrical part, we must include the Lenz electromotive voltage E_{bemf} as :

$$E_{bemf} = k_0\left(1 - \left(\frac{y+y_0}{y_{max}}()^2\right)(\dot{})\right). \tag{2.4}$$

The entire mathematical model that signifies the physical model in Figure 1 can be derived using Newton's second law and Kirchhoff's laws. It is regulated by the subsequent nonlinear differential

equations:

$$m\ddot{y} + \mu_0\dot{y} + k_0 y + k_1 y^2 + k_2 y^3 = F_C + F(\tau), \tag{2.5a}$$

$$L\ddot{q} + R\dot{q} + \frac{1}{C}q + E_{bemf} = 0, \tag{2.5b}$$

where y is the relative displacement of the mass m with inertial forces $m\ddot{y}$ and damping forces $\mu_0\dot{y}$, and k_0, k_1, k_2 remain linear and nonlinear stiffness of the electromechanical oscillator system. The coupling between the above equations is assured by nonlinear radial magnetic field. The external ground motion is expected to be stochastic or periodic $(F(\tau) = F_0 + F_1\, cos(\Omega_1\tau) + F_2 y\, cos(\Omega_2\tau))$ where F_0 is the critical amplitude, $F_1\, cos(\Omega_1\tau)$ is the external force, with amplitude F_1 and Ω_1 is the excitation frequency, $F_2 y\, cos(\Omega_2\tau)$ is the parametric force, with amplitude F_2 and Ω_2 is the excitation frequency. We put Eq (2.5) into dimensionless form by setting: $x = y/l,\ z = q/Q_0$ where Q_0 is the reference charge and l is the reference length. Let's set $\omega_e = \sqrt{\frac{1}{LC}},\ \omega_m = \sqrt{\frac{k_0}{m}}$, by the time transformation $t = \omega_e\tau$.

Dimensionless variables introduced by scaling the system using characteristic quantities. The main goal is to eliminate the physical units and simplify the equations. Then we convert (2.5) into the following

$$\omega_1 = \frac{\omega_m}{\omega_e}, \omega_2 = \frac{\omega_e}{\omega_m}, \mu_m = \frac{\mu_0}{m\omega_e}, \mu_e = \frac{R}{L\omega_e}, \lambda_1 = \frac{k_1 l}{m\omega_e^2}, \lambda_2 = \frac{k_2 l^2}{m\omega_e^2}, f_0 = F_0, f_1 = \frac{F_1}{ml\omega_e^2},$$
$$f_2 = \frac{F_2}{ml\omega_e^2}, \gamma_0 = \frac{\alpha_0 Q_0}{ml\omega_e}\left(\frac{y_0^2}{y_{\max}^2} - 1\right), \gamma_1 = \frac{2\alpha_0 y_0 Q_0}{m\omega_e y_{\max}^2}, \gamma_2 = \frac{\alpha_0 l Q_0}{m\omega_e y_{\max}^2},$$
$$\beta_0 = \frac{k_0 l}{LQ_0\omega_e}\left(1 - \frac{y_0^2}{y_{\max}^2}\right), \beta_1 = -\frac{2k_0 y_0 l^2}{LQ_0\omega_e y_{\max}^2}, \beta_2 = -\frac{k_0 l^3}{LQ_0\omega_e y_{\max}^2}.$$

We attain the resulting dimensionless equations for the present electromechanical seismograph as:

$$\ddot{x} + \mu_m\dot{x} + \omega_1^2 x + \lambda_1 x^2 + \lambda_2 x^3 + (\gamma_0 + \gamma_1 x + \gamma_2 x^2)\dot{z} = f_0 + f_1\, cos(\Omega_1 t) + f_2 x\, cos(\Omega_2 t), \tag{2.6a}$$

$$\ddot{z} + \mu_e\dot{z} + \omega_2^2 z + (\beta_0 + \beta_1 x + \beta_2 x^2)\dot{x} = 0. \tag{2.6b}$$

Assume

$$\mu_m \to \varepsilon\mu_m, \lambda_1 \to \varepsilon\lambda_1, \lambda_2 \to \varepsilon\lambda_2, \gamma_0 \to \varepsilon\gamma_0, \gamma_1 \to \varepsilon\gamma_1, \gamma_2 \to \varepsilon\gamma_2, f_0 \to \varepsilon f_0, f_1 \to$$
$$\varepsilon f_1, f_2 \to \varepsilon f_2, \mu_e \to \varepsilon\mu_e, \beta_0 \to \varepsilon\beta_0, \beta_1 \to \varepsilon\beta_1, \beta_2 \to \varepsilon\beta_2, f_3 \to \varepsilon f_3, f_4 \to \varepsilon f_4.$$

Where, ε is often used as a small perturbation parameter in the analysis of nonlinear systems. The idea is to treat ε as a small parameter and perform an asymptotic expansion or perturbation analysis. It ensures stability, smooths out nonlinearities, helps with perturbation analysis, and is crucial for ensuring that numerical methods work effectively.

So, Eq (2.6) will be written as

$$\ddot{x} + \varepsilon\mu_m\dot{x} + \omega_1^2 x + \varepsilon\lambda_1 x^2 + \varepsilon\lambda_2 x^3 + \varepsilon(\gamma_0 + \gamma_1 x + \gamma_2 x^2)\dot{z}$$

$$= \varepsilon(f_0 + f_1\, cos(\Omega_1 t) + f_2 x\, cos(\Omega_2 t)), \tag{2.7a}$$

$$\ddot{z} + \varepsilon\mu_e \dot{z} + \omega_2^2 z + \varepsilon(\beta_0 + \beta_1 x + \beta_2 x^2)\dot{x} = 0. \tag{2.7b}$$

The first oscillator x (mechanical part) is a forced Duffing oscillator related with nonlinear coupling term, and the second one z (electrical part) is a linear damped oscillator with nonlinear coupling term. $\dot{x}$, $\dot{z}$, $\ddot{x}$ and $\ddot{z}$ are the first and second derivative with respect to time t, μ_m and μ_e are linear damping coefficients, λ_1, λ_2 are non-linear parameters, ε is a small perturbation parameter where $0 < \varepsilon << 1$, f_0, f_1, f_2, f_3, f_4, are the excitation forces amplitudes (f_0, f_1, f_2 are mixed mechanical excitations and f_3, f_4 are mixed electrical excitations), ω_1, ω_2 stand the natural frequencies and $\Omega_1, \Omega_2, \Omega_3, \Omega_4$ remain the excitation frequencies, γ_j and β_j $(j = 0,1,2)$ are the coupling terms.

The modified and investigated system [11] after adding mixed excitations with new controller technique is in the following form [11]:

$$\ddot{x} + \varepsilon\mu_m \dot{x} + \omega_1^2 x + \varepsilon\lambda_1 x^2 + \varepsilon\lambda_2 x^3 + \varepsilon(\gamma_0 + \gamma_1 x + \gamma_2 x^2)\dot{z}$$
$$= \varepsilon(f_0 + f_1\, cos(\Omega_1 t) + f_2 x\, cos(\Omega_2 t)) + F_{1c}(t), \tag{2.8a}$$

$$\ddot{z} + \varepsilon\mu_e \dot{z} + \omega_2^2 z + \varepsilon(\beta_0 + \beta_1 x + \beta_2 x^2)\dot{x} = \varepsilon(f_3\, cos(\Omega_3 t) + f_4 z\, cos(\Omega_4 t)) + F_{2c}(t). \tag{2.8b}$$

$F_{1c}(t), F_{2c}(t)$ are the control inputs to reduce the vibrations that happen at principal simultaneous resonance case ($\Omega_2 \cong \omega_1, \Omega_4 \cong \omega_2$) and this optimal controller is called Nonlinear Proportional-Derivative (NPD) within Negative Cubic Velocity Feedback Controller (NCVFC) to be a resonant innovative controller (NPDVF) as in the form:

$$F_{1c}(t) = -\varepsilon(p_1 x + d_1^{\cdot} x + \alpha_1 x^3 + \alpha_2 x^2 \dot{x} + \alpha_3 x \dot{x}^2 + G_1^{\cdot} x^3), \tag{2.9a}$$

$$F_c(t) = -\varepsilon\left(p_2 z + d_2^{\cdot} z + \alpha_4 z^3 + \alpha_5 z^2 \dot{z} + \alpha_6 z \dot{z}^2 + G_2^{\cdot} z^3\right), \tag{2.9b}$$

where $-(p_1 x + d_1^{\cdot} x), -(p_2 z + d_2^{\cdot} z)$ are the linear control forces, and $-(\alpha_1 x^3 + \alpha_2 x^2 \dot{x} + \alpha_3 x \dot{x}^2)$, $-(\alpha_4 z^3 + \alpha_5 z^2 \dot{z} + \alpha_6 z \dot{z}^2)$ are the non-linear control forces, and G_1, G_2 stand the gain amounts. Figure 2 depicts the block chart of the model within the novel controller.

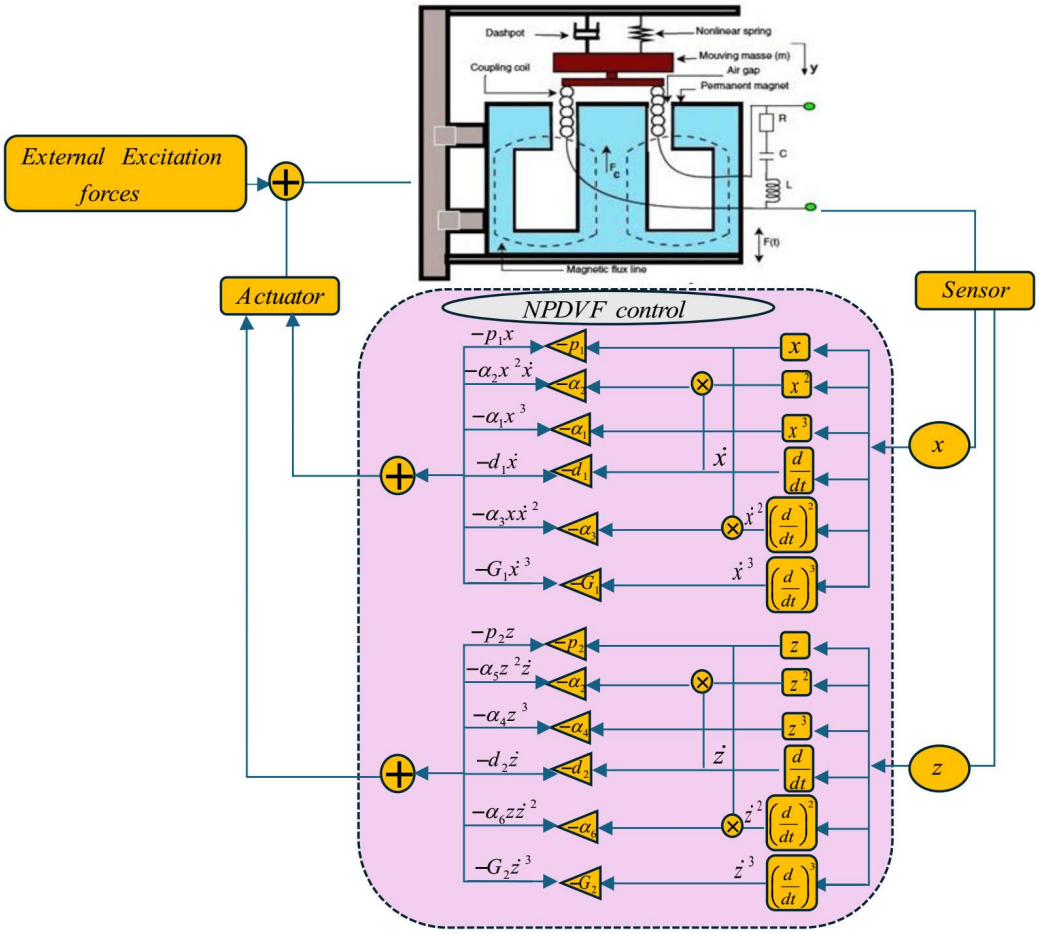

Figure 2. Block graph of the controlled electromechanical seismograph model with NPDGF controller.

3. The mathematical model study

The perturbation technique [53] is investigated here to get the following approximate solutions as follows:

$$x(t,\varepsilon) = x_0(T_0,T_1) + \varepsilon x_1(T_0,T_1) + O(\varepsilon^2), \tag{3.1a}$$

$$z(t,\varepsilon) = z_0(T_0,T_1) + \varepsilon z_1(T_0,T_1) + O(\varepsilon^2), \tag{3.1b}$$

Where, $T_0 = t$ and $T_1 = \varepsilon t$ represent time scales.

The derivatives are presented as:

$$\frac{d}{dt} = D_0 + \varepsilon D_1 + \ldots \tag{3.2a}$$

$$\frac{d^2}{dt^2} = D_0^2 + 2\varepsilon D_0 D_1 + \ldots \tag{3.2b}$$

Substituting Eq (3.1) into Eq (2.8) within Eqs (2.9, 3.2) and simply solving the expressions of the order $O(\varepsilon^0)$ and $O(\varepsilon^1)$ to be in the following relation:

$$D_0^2x_0+\omega_1^2x_0+\varepsilon\omega_1^2x_1+\varepsilon(D_0^2x_1+2D_0D_1x_0)+\varepsilon\mu_m(D_0x_0)+\varepsilon\lambda_1x_0^2+\varepsilon\lambda_2x_0^3+\varepsilon\gamma_0(D_0z_0)$$
$$+\varepsilon\gamma_1x_0(D_0z_0)++\varepsilon\gamma_2x_0^2(D_0z_0)-\varepsilon f_0-\varepsilon f_1\,cos(\Omega_1t)-\varepsilon f_2x_0\,cos(\Omega_2t)+\varepsilon p_1x_0$$
$$+\varepsilon\,d_1\,D_0\,x_0+\varepsilon\alpha_1x_0^3+\varepsilon\alpha_2\big(x_0^2(D_0x_0)\big)+\varepsilon\alpha_3x_0(D_0x_0)^2+\varepsilon\,G_1(\,D_0x_0)^3=0, \tag{3.3a}$$

$$D_0^2z_0+\omega_2^2z_0+\varepsilon\omega_2^2z_1+\varepsilon(D_0^2z_1+2D_0D_1z_0)+\varepsilon\mu_e(D_0z_0)+\varepsilon\beta_0(D_0x_0)+\varepsilon\beta_1z_0(D_0x_0)$$
$$+\varepsilon\beta_2z_0^2(D_0x_0)-\varepsilon f_3\,cos(\Omega_3t)-\varepsilon f_4z_0\,cos(\Omega_4t)+\varepsilon p_2z_0+\varepsilon\,d_2\,D_0\,z_0+\varepsilon\alpha_4z_0^3$$
$$+\varepsilon\alpha_5\big(z_0^2(D_0z_0)\big)+\varepsilon\alpha_6z_0(D_0z_0)^2+\varepsilon\,G_2(\,D_0z_0)^3=0. \tag{3.3b}$$

Connecting terms of the same order of ε in Eq (3.3) to get:

$$O(\varepsilon^0)\colon (D_0^2+\omega_1^2)x_0=0, \tag{3.4a}$$
$$(D_0^2+\omega_2^2)z_0=0, \tag{3.4b}$$
$$O(\varepsilon^1)\colon (D_0^2+\omega_1^2)x_1=-2D_0D_1x_0-\mu_mD_0x_0-\lambda_1x_0^2-\lambda_2x_0^3-\gamma_0D_0z_0-\gamma_1x_0(D_0z_0)$$
$$-\gamma_2x_0^2(D_0z_0)+f_0+f_1\,cos(\Omega_1t)+f_2x_0\,cos(\Omega_2t)-p_1x_0-d_1(D_0x_0)-\alpha_1x_0^3$$
$$-\alpha_2x_0^2(D_0x_0)-\alpha_3x_0(D_0x_0)^2-G_1(\,D_0x_0)^3, \tag{3.5a}$$
$$(D_0^2+\omega_2^2)z_1=-2D_0D_1z_0-\mu_eD_0z_0-\beta_0D_0x_0-\beta_1z_0(D_0x_0)-\beta_2z_0^2(D_0x_0)$$
$$+f_3\,cos(\Omega_3t)+f_4z_0\,cos(\Omega_4t)-p_2z_0-d_2(D_0z_0)$$
$$-\alpha_4z_0^3-\alpha_5z_0^2(D_0z_0)-\alpha_6z_0(D_0z_0)^2-G_2(\,D_0z_0)^3. \tag{3.5b}$$

The solution for Eq (3.4) is

$$x_0=A_1(T_1)e^{i\omega_1T_0}+\bar{A}_1(T_1)e^{-i\omega_1T_0}, \tag{3.6a}$$
$$z_0=B_1(T_1)e^{i\omega_2T_0}+\bar{B}_1(T_1)e^{-i\omega_2T_0}. \tag{3.6b}$$

Substituting Eq (3.6) into Eq (3.5) yields

$$(D_0^2+\omega_1^2)x_1=\begin{pmatrix}-2i\omega_1D_1A_1-i\omega_1\mu_mA_1-3\lambda_2A_1^2\bar{A}_1+\frac{1}{2}f_2\bar{A}_1e^{i(\Omega_2-2\omega_1)T_0}\\-p_1A_1-i\omega_1d_1A_1-3\alpha_1A_1^2\bar{A}_1-2i\omega_1\alpha_2A_1^2\bar{A}_1\\-\alpha_3\omega_1^2A_1^2\bar{A}_1-3iG_1\omega_1^3A_1^2\bar{A}_1\end{pmatrix}e^{i\omega_1T_0}+NST+cc, \tag{3.7a}$$

$$(D_0^2+\omega_2^2)z_1=\begin{pmatrix}-2i\omega_2D_1B_1-i\omega_2\mu_eB_1+\frac{1}{2}f_4\bar{B}_1e^{i(\Omega_4-\omega_2)T_0}\\-p_2B_1-i\omega_2d_2B_1-3\alpha_4B_1^2\bar{B}_1-2i\omega_2\alpha_5B_1^2\bar{B}_1\\-\alpha_6\omega_2^2B_1^2\bar{B}_1-3iG_2\omega_2^3B_1^2\bar{B}_1\end{pmatrix}e^{i\omega_2T_0}+NST+cc, \tag{3.7b}$$

where cc represents the complex conjugate of the preceding parameters, NST signifies non-secular terms. By means of primary parametric resonance case $\Omega_2\cong\omega_1,\Omega_4\cong\omega_2$, the frequency detuning parameters σ_1,σ_2 for the parametric excitation frequency considered by

$$\Omega_2 \cong \omega_1 + \varepsilon\sigma_1, \Omega_4 \cong \omega_2 + \varepsilon\sigma_2. \tag{3.8}$$

In Eq (3.7), the solvability conditions produce when terms of secular terms are cancelled via Eq (3.8). Bearing in mind Eq (3.8), removing the secular terms in Eq (3.7) we get:

$$-2i\omega_1 D_1 A_1 - i\omega_1\mu_m A_1 - 3\lambda_2 A_1^2\bar{A}_1 + \frac{1}{2}f_2\bar{A}_1 e^{i\sigma_1 T_1} - p_1 A_1 - i\omega_1 d_1 A_1$$

$$-3\alpha_1 A_1^2\bar{A}_1 - i\omega_1\alpha_2 A_1^2\bar{A}_1 - \alpha_3\omega_1^2 A_1^2\bar{A}_1 - 3iG_1\omega_1^3 A_1^2\bar{A}_1 = 0, \tag{3.9a}$$

$$-2i\omega_2 D_1 B_1 - i\omega_2\mu_e B_1 + \frac{1}{2}f_4\bar{B}_1 e^{i\sigma_2 T_0} - p_2 B_1 - i\omega_2 d_2 B_1 - 3\alpha_4 B_1^2\bar{B}_1$$

$$-i\omega_2\alpha_5 B_1^2\bar{B}_1 - \alpha_6\omega_2^2 B_1^2\bar{B}_1 - 3iG_2\omega_2^3 B_1^2\bar{B}_1 = 0. \tag{3.9b}$$

To distinct the averaging conditions that manage the elements of Eq (3.9), let definite A_1, B_1 and $\bar{A}_1, \bar{B}_1$ are expressed in the next polar expressions

$$A_1 = \tfrac{1}{2}a_1(T_1)e^{i\theta_1(T_1)},\ \bar{A}_1 = \tfrac{1}{2}a_1(T_1)e^{-i\theta_1(T_1)}, \tag{3.10a}$$

$$B_1 = \tfrac{1}{2}a_2(T_1)e^{i\theta_2(T_1)},\ \bar{B}_1 = \tfrac{1}{2}a_2(T_1)e^{-i\theta_2(T_1)}, \tag{3.10b}$$

where a_1, a_2 and θ_1, θ_2 stand the steady-state amplitudes and phases, respectively. Substitute Eq (3.10) in Eq (3.9), we acquire:

$$-i\omega_1 a_1^{'} + \frac{1}{2}\omega_1 a_1(\sigma_1 - \gamma_1^{'}) - \frac{1}{2}i\omega_1\mu_m a_1 - \frac{3}{8}\lambda_2 a_1^3 + \frac{1}{4}a_1 f_2(\cos\gamma_1 + i\sin\gamma_1)$$

$$-\tfrac{1}{2}p_1 a_1 - \tfrac{1}{2}i\omega_1 d_1 a_1 - \tfrac{3}{8}\alpha_1 a_1^3 - \tfrac{1}{8}i\omega_1\alpha_2 a_1^3 - \tfrac{1}{8}\alpha_3\omega_1^2 a_1^3 - \tfrac{3}{8}iG_1\omega_1^3 a_1^3 = 0, \tag{3.11a}$$

$$-i\omega_2 a_2^{'} + \frac{1}{2}\omega_2 a_2(\sigma_2 - \gamma_2^{'}) - \frac{1}{2}i\omega_2\mu_e a_1 + \frac{1}{4}a_2 f_4(\cos\gamma_2 + i\sin\gamma_2) - \frac{1}{2}p_2 a_2$$

$$-\tfrac{1}{2}i\omega_2 d_2 a_2 - \tfrac{3}{8}\alpha_4 a_2^3 - \tfrac{1}{8}i\omega_2\alpha_5 a_2^3 - \tfrac{1}{8}\alpha_6\omega_2^2 a_2^3 - \tfrac{3}{8}iG_2\omega_2^3 a_2^3 = 0, \tag{3.11b}$$

where $\gamma_1 = \sigma_1 T_1 - 2\theta_1,\ \gamma_2 = \sigma_2 T_1 - 2\theta_2$, then separating real and imaginary elements:

$$a_1^{'} = \tfrac{1}{2}\left[-d_1 - \mu_m + \tfrac{1}{2\omega_1}f_2\sin\gamma_1\right]a_1 - \tfrac{1}{8}[\alpha_2 + 3G_1\omega_1^2]a_1^3, \tag{3.12a}$$

$$a_1\gamma_1^{'} = \left[\sigma_1 + \tfrac{1}{2\omega_1}f_2\cos\gamma_1 - \tfrac{p_1}{\omega_1}\right]a_1 - \tfrac{1}{4}\left[\tfrac{3}{\omega_1}\lambda_2 + \tfrac{3}{\omega_1}\alpha_1 + \alpha_3\omega_1\right]a_1^3, \tag{3.12b}$$

$$a_2^{'} = \tfrac{1}{2}\left[-d_2 - \mu_e + \tfrac{1}{2\omega_2}f_4\sin\gamma_2\right]a_2 - \tfrac{1}{8}[\alpha_5 + 3G_2\omega_2^2]a_2^3, \tag{3.13a}$$

$$a_2\gamma_2^{'} = \left[\sigma_2 + \tfrac{1}{2\omega_2}f_4\cos\gamma_2 - \tfrac{p_2}{\omega_2}\right]a_2 - \tfrac{1}{4}\left[\tfrac{3}{\omega_2}\alpha_4 + \alpha_6\omega_2\right]a_2^3. \tag{3.13b}$$

For steady-state responses ($a_1^{'} = a_2^{'} = \gamma_1^{'} = \gamma_2^{'} = 0$), the periodic solution resultant to Eqs (3.12) and (3.13) are given as:

$$\left[-d_1 - \mu_m + \frac{1}{2\omega_1} f_2 \sin\gamma_1\right] a_1 - \frac{1}{4}[\alpha_2 + 3G_1\omega_1^2]a_1^3 = 0, \tag{3.14a}$$

$$\left[\sigma_1 + \frac{1}{2\omega_1} f_2 \cos\gamma_1 - \frac{p_1}{\omega_1}\right] a_1 - \frac{1}{4}\left[\frac{3}{\omega_1}\lambda_2 + \frac{3}{\omega_1}\alpha_1 + \alpha_3\omega_1\right] a_1^3 = 0, \tag{3.14b}$$

$$\left[-d_2 - \mu_e + \frac{1}{2\omega_2} f_4 \sin\gamma_2\right] a_2 - \frac{1}{4}[\alpha_5 + 3G_2\omega_2^2]a_2^3 = 0, \tag{3.15a}$$

$$\left[\sigma_2 + \frac{1}{2\omega_2} f_4 \cos\gamma_2 - \frac{p_2}{\omega_2}\right] a_2 - \frac{1}{4}\left[\frac{3}{\omega_2}\alpha_4 + \alpha_6\omega_2\right] a_2^3 = 0. \tag{3.15b}$$

The Newton-Raphson method and MATLAB software are used to determine the steady-state answers from the algebraic equations. The Lyapunov first approach is used to determine the right-hand side eigenvalues of the Jacobian matrix at Eqs. (3.15) to calculate the stability of the steady-state shell system.

$$\begin{bmatrix} a_1^{'} \\ \gamma_1^{'} \\ a_2^{'} \\ \gamma_2^{'} \end{bmatrix} = \begin{bmatrix} R_{11} & R_{12} & R_{13} & R_{14} \\ R_{21} & R_{22} & R_{23} & R_{24} \\ R_{31} & R_{32} & R_{33} & R_{34} \\ R_{41} & R_{42} & R_{43} & R_{44} \end{bmatrix} \begin{bmatrix} a_1 \\ \gamma_1 \\ a_2 \\ \gamma_2 \end{bmatrix}, \tag{3.16}$$

where

$$R_{11} = \frac{\partial a_1'}{\partial a_1} = \frac{1}{2}\left[-d_1 - \mu_m + \frac{1}{2\omega_1} f_2 \sin\gamma_1\right] - \frac{3}{8}\left[\alpha_2 + 3G_1\omega_1^2\right]a_1^2,$$

$$R_{12} = \frac{\partial a_1^{'}}{\partial \gamma_1} = \frac{1}{4\omega_1} a_1 f_2 \cos\gamma_1,$$

$$R_{13} = \frac{\partial a_1^{'}}{\partial a_2} = 0,$$

$$R_{14} = \frac{\partial a_1^{'}}{\partial \gamma_2} = 0,$$

$$R_{21} = \frac{\partial \gamma_1^{'}}{\partial a_1} = \frac{1}{a_1}\left[\sigma_1 + \frac{1}{2\omega_1} f_2 \cos\gamma_1 - \frac{p_1}{\omega_1}\right] - \frac{3}{4}\left[\frac{3}{\omega_1}\lambda_2 + \frac{3}{\omega_1}\alpha_1 + \alpha_3\omega_1\right] a_1,$$

$$R_{22} = \frac{\partial \gamma_1^{'}}{\partial \gamma_1} = -\frac{1}{2\omega_1} f_2 \sin\gamma_1,$$

$$R_{23} = \frac{\partial \gamma_1^{'}}{\partial a_2} = 0,$$

$$R_{24} = \frac{\partial \gamma_1^{'}}{\partial \gamma_2} = 0,$$

$$R_{31} = \frac{\partial a_2^{'}}{\partial a_1} = 0, R_{32} = \frac{\partial a_2^{'}}{\partial \gamma_1} = 0,$$

$$R_{13} = \frac{\partial a_2^{'}}{\partial a_2} = \frac{1}{2}\left[-d_2 - \mu_e + \frac{1}{2\omega_2} f_4 \sin\gamma_2\right] - \frac{3}{8}[\alpha_5 + 3G_2\omega_2^2]a_2^2,$$

$$R_{14} = \frac{\partial a_2^{'}}{\partial \gamma_2} = \frac{1}{4\omega_2} a_2 f_4 \cos\gamma_2,$$

$$R_{41} = \frac{\partial \gamma_2^{'}}{\partial a_1} = 0,$$

$$R_{42} = \frac{\partial \gamma_2^{'}}{\partial \gamma_1} = 0,$$

$$R_{43} = \frac{\partial \gamma_2^{'}}{\partial a_2} = \frac{1}{a_2}\left[\sigma_2 + \frac{1}{2\omega_2} f_4 \cos\gamma_2 - \frac{p_2}{\omega_2}\right] - \frac{3}{4}\left[\frac{3}{\omega_2}\alpha_4 + \alpha_6\omega_2\right]a_2,$$

$$R_{44} = \frac{\partial \gamma_2^{'}}{\partial \gamma_2} = -\frac{1}{2\omega_2} f_4 \sin\gamma_2.$$

To determine the controlled model's stable zones, calculate the following determinant in the previous matrix.

$$\begin{vmatrix} R_{11} - \lambda & R_{12} & 0 & 0 \\ R_{21} & R_{22} - \lambda & 0 & 0 \\ 0 & 0 & R_{33} - \lambda & R_{34} \\ 0 & 0 & R_{43} & R_{44} - \lambda \end{vmatrix} = 0. \tag{3.17}$$

Then,

$$\lambda^4 + r_1\lambda^3 + r_2\lambda^2 + r_3\lambda + r_4 = 0. \tag{3.18}$$

Where, λ designates the Jacobian matrix's eigenvalue,

$$r_1 = -R_{11} - R_{22} - R_{33} - R_{44},$$

$$r_2 = R_{11}R_{22} + R_{11}R_{33} + R_{11}R_{44} + R_{22}R_{33} + R_{22}R_{44} + R_{33}R_{44} - R_{12}R_{21} - R_{34}R_{43},$$

$$r_3 = R_{12}R_{21}R_{33} + R_{12}R_{21}R_{44} + R_{11}R_{34}R_{43} + R_{22}R_{34}R_{43}$$
$$-R_{11}R_{22}R_{33} - R_{11}R_{22}R_{44} - R_{11}R_{33}R_{44} - R_{22}R_{33}R_{44},$$
$$r_4 = R_{11}R_{22}R_{33}R_{44} + R_{12}R_{21}R_{34}R_{43} - R_{11}R_{22}R_{34}R_{43} - R_{12}R_{21}R_{33}R_{44}$$

are the coefficient of Eq (3.18).

Routh-Hurwitz criterion is used to examine the stability of equilibrium solutions via discovering sufficient and necessary requirements to be stable are:

$$r_1 > 0, r_1r_2 - r_3 > 0, r_3(r_1r_2 - r_3) - r_1^2r_4 > 0, r_4 > 0. \tag{3.19}$$

Furthermore, to conclude the nature of the roots of Eq (3.18), we define the following discriminants $\Delta, \Delta_0, \Delta_1, \Delta_2$, and Δ_3 [58,59] as:

$$\Delta = 256r_4^3 - 192r_1r_3r_4^2 - 128r_2^2r_4^2 + 144r_2r_3^2r_4 - 27r_3^4 + 144r_1^2r_2r_4^2 - 6r_1^2r_3^2r_4 - 80r_1r_2^2r_3r_4$$
$$+18r_1r_2r_3^3 + 16r_2^4r_4 - 4r_2^3r_3^2 - 27r_1^4r_4^2 + 18r_1^3r_2r_3r_4 - 4r_1^3r_3^3 - 4r_1^2r_2^3r_4 + r_1^2r_2^2r_3^2$$
$$\Delta_0 = 8r_3 - 3r_1^2, \Delta_1 = r_1^3 + 8r_3^2 - 4r_1r_2, \Delta_2 = r_2^2 - 3r_1r_3 + 12r_4,$$
$$\Delta_3 = 64r_4 - 16r_2^2 + 16r_1^2r_2 - 16r_1r_3 - 3r_1^4.$$

By joining the conditions Eq (3.19) with each one of the following possible cases, one can establish the sort of roots of Eq (3.18) as:

a) If $\Delta < 0$ then the equation has two different real and two complex conjugate roots.
b) If $\Delta > 0$, then either the four roots are all complex conjugate or real according to the subsequent two cases:
   i. If $\Delta_0 < 0$ and $\Delta_3 < 0$ then all four roots are different and real.
   ii. If $\Delta_0 > 0$ or if $\Delta_3 > 0$ then the roots are two pairs of complex conjugates.
c) If $\Delta = 0$ then the system has multiple roots according to the following four cases:
   i. If $\Delta_0 < 0$, $\Delta_3 < 0$ and $\Delta_2 \neq 0$, there are two real simple roots and a real double roots
   ii. If $\Delta_3 > 0$ or ($\Delta_0 > 0$ and ($\Delta_3 \neq 0$ or $\Delta_1 \neq 0$)), there are two complex conjugate roots and two real equal roots.
   iii. If $\Delta_2 = 0$ and $\Delta_3 \neq 0$, there are three real equal roots and one real different root.
   iv. If $\Delta_3 = 0$, at that time:
      1- If $\Delta_0 < 0$, there are two real double roots.
      2- If $\Delta_0 > 0$ and $\Delta_1 = 0$, the roots be present two double complex conjugate roots.
      3- If $\Delta_2 = 0$, all four roots are equal to $-\frac{r_1}{4}$.

4. The optimum control parameters

The mechanism of the NPDVF controller at the measured simultaneous resonance can be clarified with the aid of Eqs (3.12) and (3.13). It is clear from Eqs (3.12) and (3.13) that the addition of the NPDVF controller to the considered framework has modified the linear damping terms μ_m and μ_e to the controlled terms $\mu_{m-control}$ and $\mu_{e-control}$. Moreover, the detuning parameter σ_1 and σ_2 is modified to $\sigma_{1-control}$ and $\sigma_{2-control}$, where $\mu_{m-control}$, $\mu_{e-control}$, $\sigma_{1-control}$, and $\sigma_{2-control}$ are given as follows:

$$\mu_{m-control} = -\frac{1}{2}(\mu_m + d_1), \tag{4.1}$$

$$\sigma_{1-control} = \left(\sigma_1 - \frac{p_1}{2\omega_1}\right), \tag{4.2}$$

$$\mu_{e-control} = -\frac{1}{2}(\mu_e + d_2), \tag{4.3}$$

$$\sigma_{2-control} = \left(\sigma_2 - \frac{p_2}{2\omega_2}\right). \tag{4.4}$$

It is clear from Eqs (4.1)–(4.4) that $\mu_{m-control}$, $\mu_{e-control}$, $\sigma_{1-control}$, and $\sigma_{2-control}$ are periodic functions on the controller, where the controlled system has the equivalent linear damping coefficients $\mu_{m-control} = -\frac{1}{2}(\mu_m + d_1)$, $\mu_{e-control} = -\frac{1}{2}(\mu_e + d_2)$ and the detuning parameters $\sigma_{1-control} = \left(\sigma_1 - \frac{p_1}{2\omega_1}\right) = \Omega_2 - \left(\omega_1 + \frac{p_1}{2\omega_1}\right)$, $\sigma_{2-control} = \left(\sigma_2 - \frac{p_2}{2\omega_2}\right) = \Omega_4 - \left(\omega_2 + \frac{p_2}{2\omega_2}\right)$. This means that the linear control forces p_1 and p_2 are responsible for changing the system natural frequencies ω_1 and ω_2, while the velocity gain d_1 and d_2 is responsible for modifying the system linear damping coefficients μ_m and μ_e. Consequently, to develop the vibration suppression efficiency of the measured scheme, the linear control forces p_1, p_2 and d_1, d_2 should be designated in a way that maximizes the objective function $\mu_{m-control}$, $\mu_{e-control}$, $\sigma_{1-control}$ and $\sigma_{2-control}$. By comparing the obtained results in Figures 8(b) and 9(a) with the objective function given by Eqs (4.1)–(4.4), we can notice that the best vibration suppression condition has occurred at the maximum values of function $\mu_{m-control}$, $\mu_{e-control}$, $\sigma_{1-contro}$ and $\sigma_{2-control}$ as summarized in Table 1.

Table 1. Optimum control parameters.

Figure	p_1	p_2	d_1	d_2	ω_1	ω_2	$\mu_{m-control} = \frac{1}{2}(\mu_m + d_1)$	$\sigma_{1-control} = \left(\sigma_1 - \frac{p_1}{2\omega_1}\right)$	$\mu_{e-control} = \frac{1}{2}(\mu_e + d_2)$	$\sigma_{2-control} = \left(\sigma_2 - \frac{p_2}{2\omega_2}\right)$	Max $\mu_{m-contro}$	Max $\mu_{e-control}$	Max $\sigma_{1-control}$	Max $\sigma_{2-control}$
16	-0.5	0	0	0	5.05	4.05	0.5 $(\mu_m + 0)$	$\sigma_1 + \frac{0.5}{2(5.05)}$	0.5 $(\mu_e + 0)$	$\sigma_2 + 0$	0.0155	0.2	1.05	1.0
24	0	-0.5	0	0	5.05	4.05	0.5 $(\mu_m + 0)$	$\sigma_1 + 0$	0.5 $(\mu_e + 0)$	$\sigma_2 + \frac{0.5}{2(4.05)}$	0.0155	0.2	1.0	1.06
17	0	0	2.5	0	5.05	4.05	0.5 $(\mu_m + 2.5)$	$\sigma_1 + 0$	0.5 $(\mu_e + 0)$	$\sigma_2 + 0$	1.2655	0.2	1.0	1.0
25	0	0	0	0.5	5.05	4.05	0.5 $(\mu_m + 0)$	$\sigma_1 + 0$	0.5 $(\mu_e + 0.5)$	$\sigma_2 + 0$	0.0155	0.45	1.0	1.0

The table 1 provides a list or summary of the important variables that were considered in the design process. The choice of each parameter was guided by the system's functional requirements and manufacturing constraints to avoid unstable regions of the system. This approach avoids pushing the system into regions that might otherwise lead to increased costs, manufacturing difficulties, or operational instability. The parameters listed in Tab. 1 are critical to the overall design of the system. Each of these variables was carefully chosen to balance the system's functional requirements with the practical limitations imposed by manufacturing capabilities.

To improve the system's response, Eqs (4.1)–(4.4) introduce more sophisticated feedback mechanisms, specifically designed to manage these nonlinearities and provide better stabilization and vibration suppression. The enhanced NPDVF controller improves the system's ability to avoid resonance conditions or mitigate their effects. The improvement of the NPDCVF controller represented by Eqs (4.1)–(4.4) is essential for addressing the nonlinear dynamics, feedback instability, and resonance issues in systems with both mechanical and electrical components. The combination of these equations allows the NPDVF controller to anticipate future disturbances, adjust for system nonlinearities, and optimize control actions in real time.

5. Results and discussions

5.1 Numerical simulation with time history

The nonlinear dynamical structure was just demonstrated by Eq (3.10) through (3.14) above. The MATLAB®18 computer programmer was then used to numerically simulate three distinct control strategies (PD, NCVF, and NPDVF) to identify which controller would minimise the destructive vibrations caused during work of the model. Figures 3–6 are plotted to appear the time history of the worst resonance case before and after using various controllers via the following values of the parameters:

$$\mu_m = 0.031, \omega_1 = 5.05, \lambda_1 = 0.00315, \lambda_2 = 0.025,$$

$$\gamma_0 = -0.2, \gamma_1 = -0.0015, \gamma_2 = 0.035, f_0 = 1.2, f_1 = 3.5,$$

$$f_2 = 4.7, \Omega_1 = 3.75, \Omega_2 = \omega_1, \mu_e = 0.4, \omega_2 = 4.05,$$

$$\beta_0 = 0.0072, \beta_1 = 0.005, \beta_2 = 0.0015, f_3 = 1.6, f_4 = 3.1,$$

$$\Omega_3 = 2.45, \Omega_4 = \omega_2, p_1 = 2.3, d_1 = 2.5,$$

$$\alpha_1 = 0.09, \alpha_2 = 0.04, \alpha_3 = 0.4, G_1 = 0.5, p_2 = 1.9, d_2 = 0.5,$$

$$\alpha_4 = 0.05, \alpha_5 = 0.03, \alpha_6 = 0.2, G_2 = 0.4, \varepsilon = 0.5,$$

with the initial conditions $x(0) = 0.5,\ \dot{x}(0) = 0,\ z(0) = 0.5,\ \dot{z}(0) = 0.$

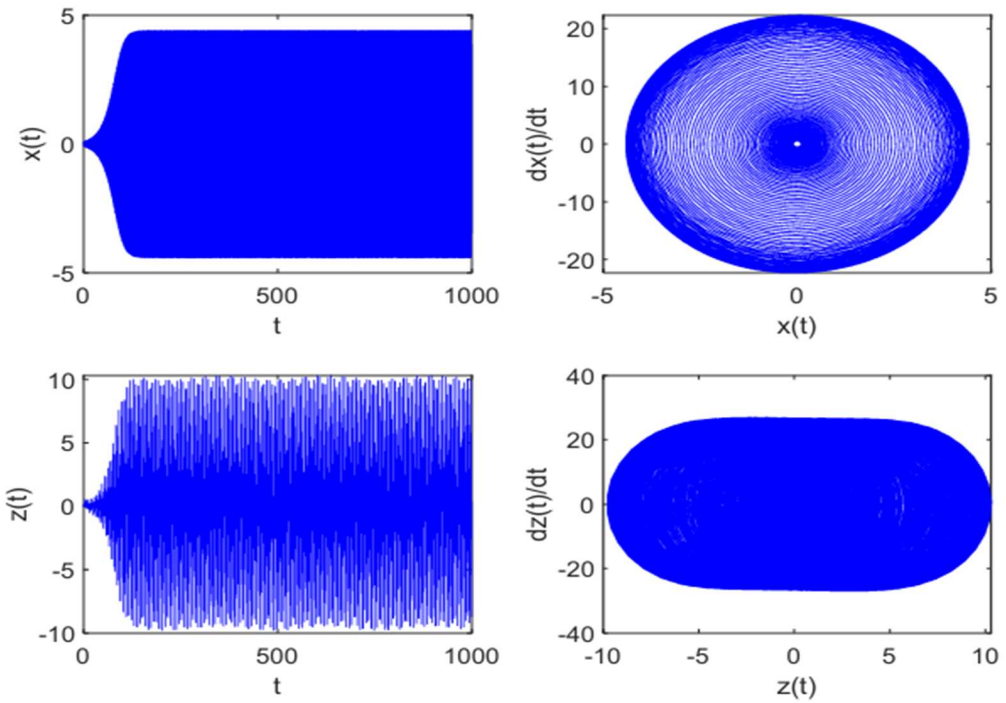

Figure 3. The measured simultaneous resonance instance ($\Omega_2 \cong \omega_1, \Omega_4 \cong \omega_2$) without controller.

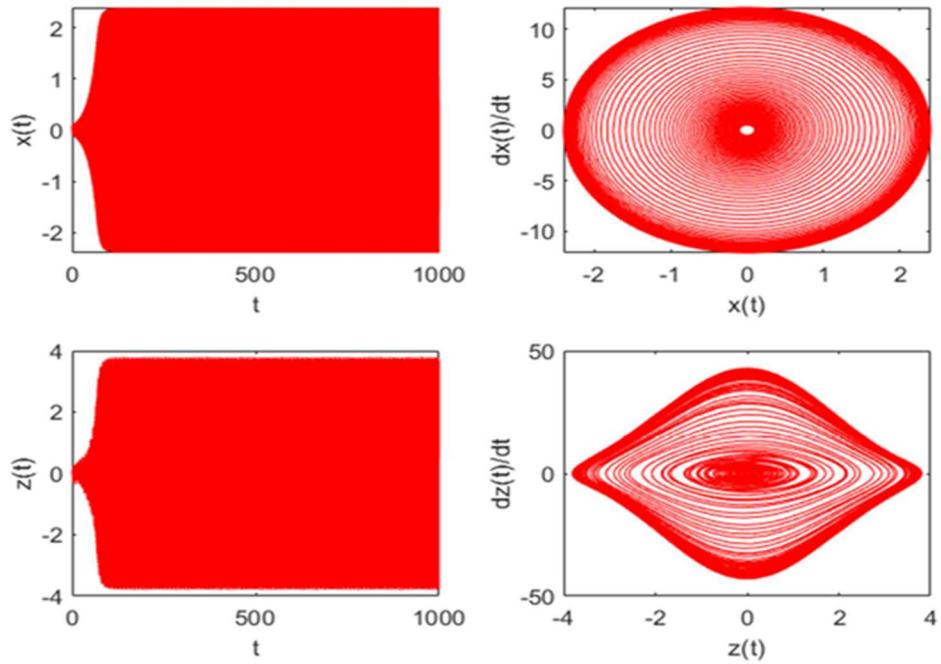

Figure 4. The measured simultaneous resonance instance ($\Omega_2 \cong \omega_1, \Omega_4 \cong \omega_2$) with PD controller.

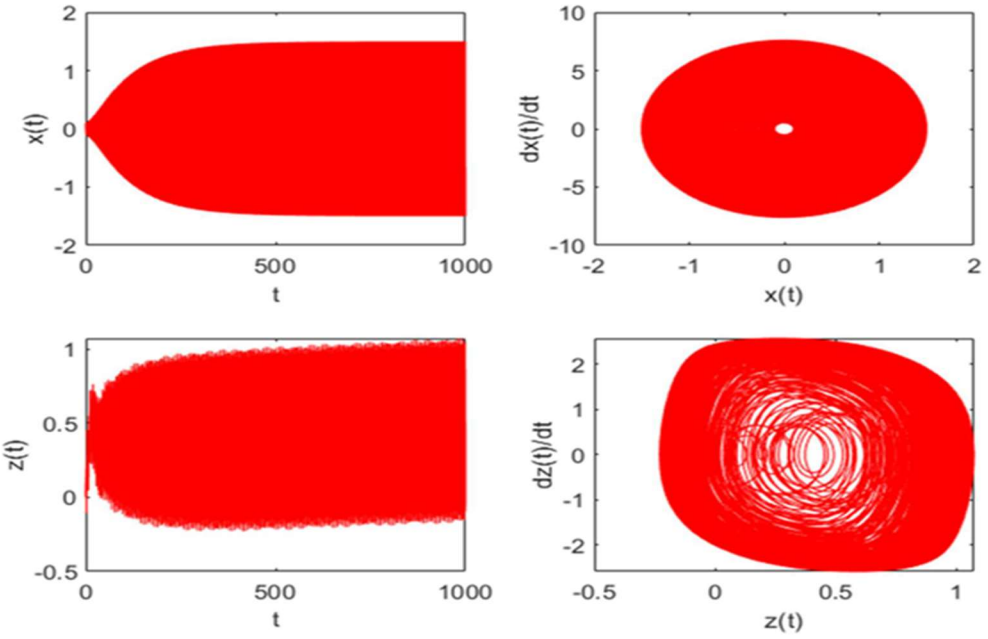

Figure 5. The measured simultaneous resonance instance ($\Omega_2 \cong \omega_1, \Omega_4 \cong \omega_2$) with NCVF controller.

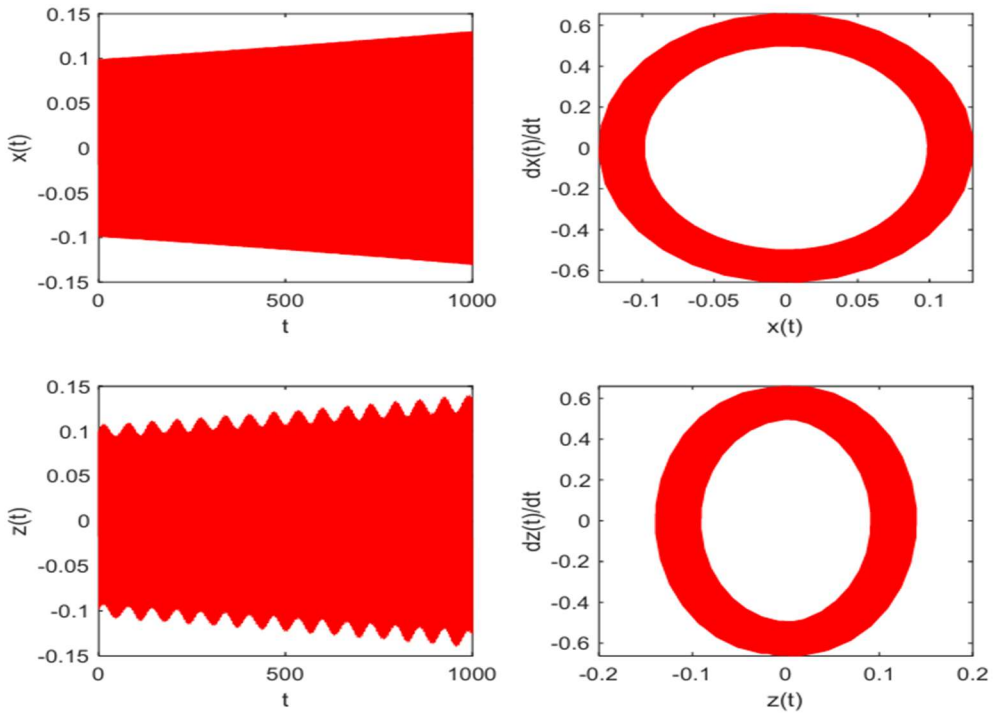

Figure 6. The measured simultaneous resonance instance ($\Omega_2 \cong \omega_1, \Omega_4 \cong \omega_2$) with the novel resonant controller NPDVF.

Figure 3 presents the basic steady-state amplitudes $x(t)$ and $z(t)$ without controller at the simultaneous resonance situation $\Omega_2 \cong \omega_1, \Omega_4 \cong \omega_2$ as the worst resonance case of the system. Figures 4–6 show the results of adding the measured controllers (PD-NCVF-NPDCVF), enabling you to indicate the best one for reducing the high vibration amplitudes. After checking, we found that the best one controller is NPDVF as it reduces the vibrations at the measured resonance in a short time. The new controller NPDCVFC is the most efficient, according to these diagrams (3–6). The controller for the observed model's active vibration is developed in this part (refer to Figure 6). The NPD and NCVFC algorithms are used for active vibration control, as mentioned earlier. With this controller rule, the depreciation rate's are enhanced for this structural model. It is obvious that the infinite norm of vibration amplitudes might be reduced with this straightforward method. The outcomes demonstrate how well the optimization strategy reduced vibrations and how quickly suitably positioned actuators and sensors were able to reduce vibrations in the model. Thus, we will select and statistically evaluate the controlled model in order to study it and examine the impact of various controlled parameters on the system.

5.2 Simulation of stability and the influence of various controlled model factors

This part examined the effects of different parameters used the regulated model in Eqs (3.14-3.15), numerically illustrated the stable and unstable areas. The beneficial case is examined to acquire a significant quantity of parameter effects. As illustrated in Figures 7–26, all curves display only stable segments without any instability areas when NPDVF controller is applied to the system. This provides an additional justification for adding this supplementary controller to the system, which is a beneficial outcome for any vibrating system. Solid curves indicate stable reactions. The solid line (——) illustrates the stable regions. Figures 7 and 19 describe the performance of the amplitude-frequency response steady-state response curves a_1 versus σ_1 and a_2 versus σ_2, respectively, with nonstable regions, which shows only stable zones. As the linear damping coefficients μ_m, μ_e decreased the amplitudes a_1, a_2 are increased and the stability region is increased as appeared in Figures 8, 20. By way of the excitation frequencies ω_1, ω_2 are increased the steady-state amplitudes a_1, a_2 are increased and all regions are stable as exposed in Figures 9, 10, 21. Moreover, the diagrams of the nonlinear control coefficient α_2 is slightly monotonic decreasing with no instability regions as depicted in Figure 11. Moreover, when the amplitudes a_1, a_2 are decreased the nonlinear control parameter α_3 is increased as illustrated in Figures 12, 22. Also, the nonlinear coefficient α_4 is monotonic decreasing in which when it decreased, the amplitude a_1 increased as shown in Figure 13. Also, as the parametric force coefficients f_2, f_4 are increased, then the steady-state amplitudes a_1, a_2 are increased with increasing in stability regions as displayed in Figures 14, 15 and 23. Besides, the curve of the linear control force coefficients p_1, p_2 are shifted to right (S.R) when the values of parameters p_1, p_2 are increased with no instability regions as graphed in Figures 16 and 24. On other hand, when the linear control force coefficients d_1 is increased, the steady-state amplitudes a_1, a_2 are increased and all zones are stable as labelled in Figures 17 and 25. In the last, as the gain coefficients G_1, G_2 increased the steady-state amplitudes a_1, a_2 are small with stability regions which are presented in Figures 18 and 26.

As listed in the figures, in which, M.I refers to monotonic increasing and M.D refers to monotonic decreasing

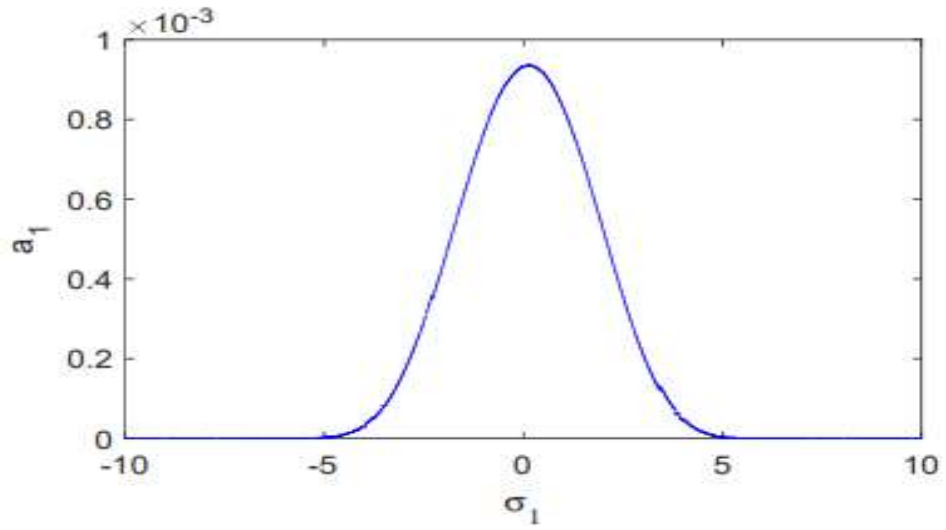

Figure 7. Response curve via a_1 versus σ_1 of the controlled structure.

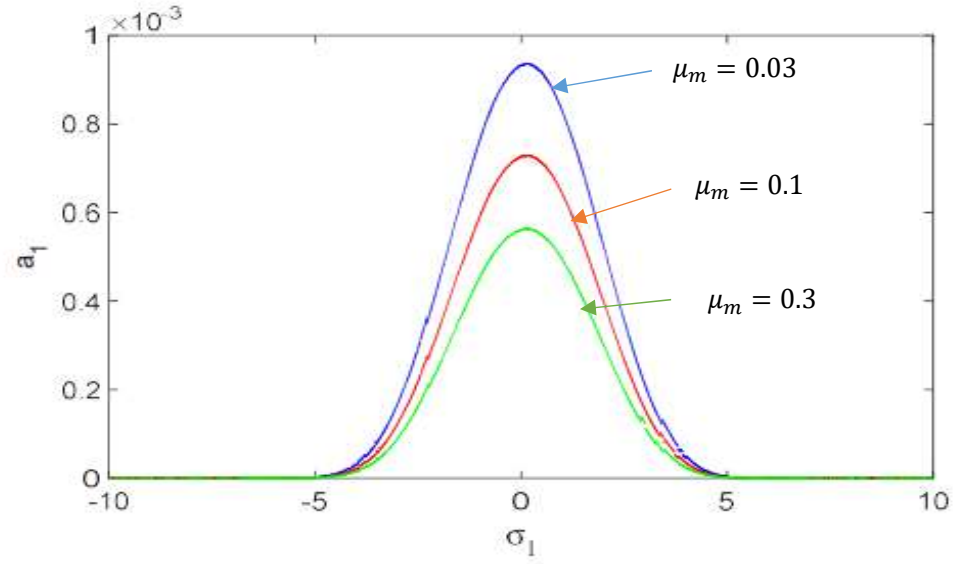

Figure 8. Impact of damping coefficient μ_m (M.D).

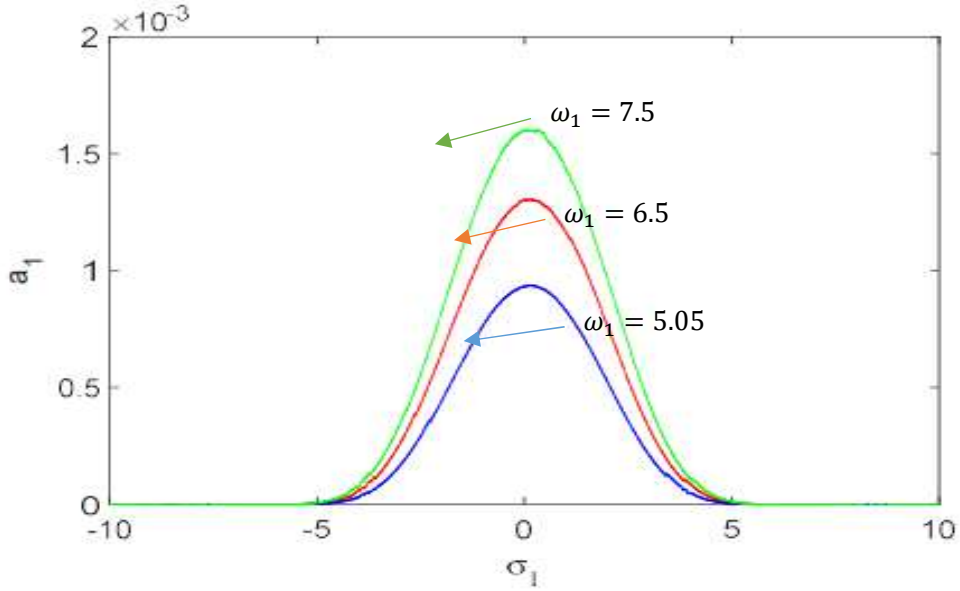

Figure 9. Effect of excitation frequency ω_1 (M.I).

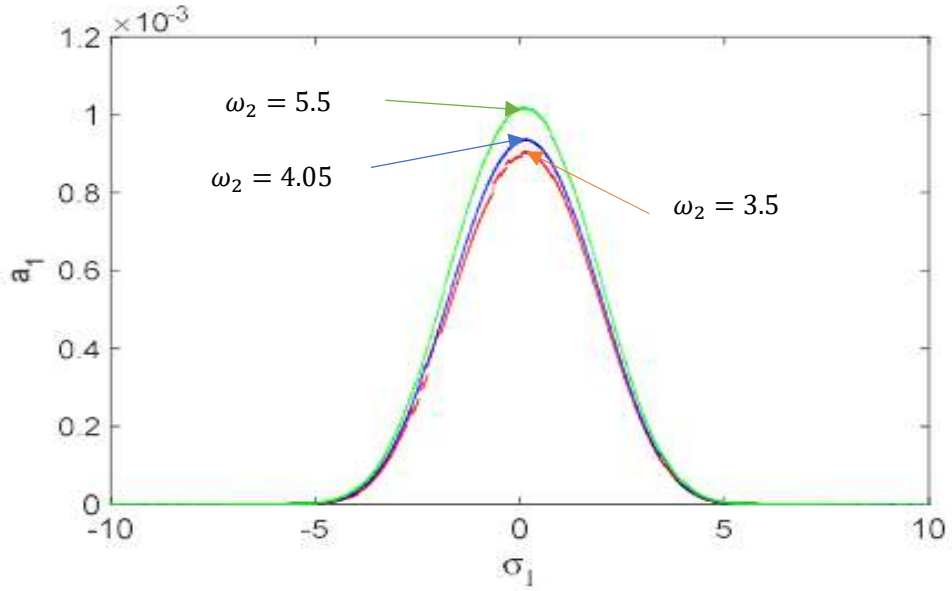

Figure 10. Influence of excitation frequency ω_2 (S.M.I) slightly monotonic Increasing.

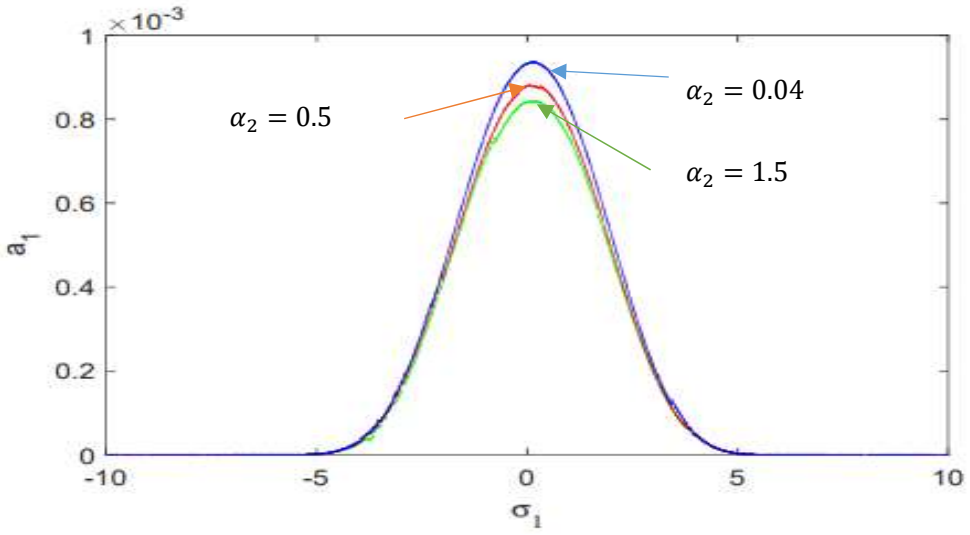

Figure 11. Influence of nonlinear control parameter α_2 (S.M.D) slightly monotonic decreasing.

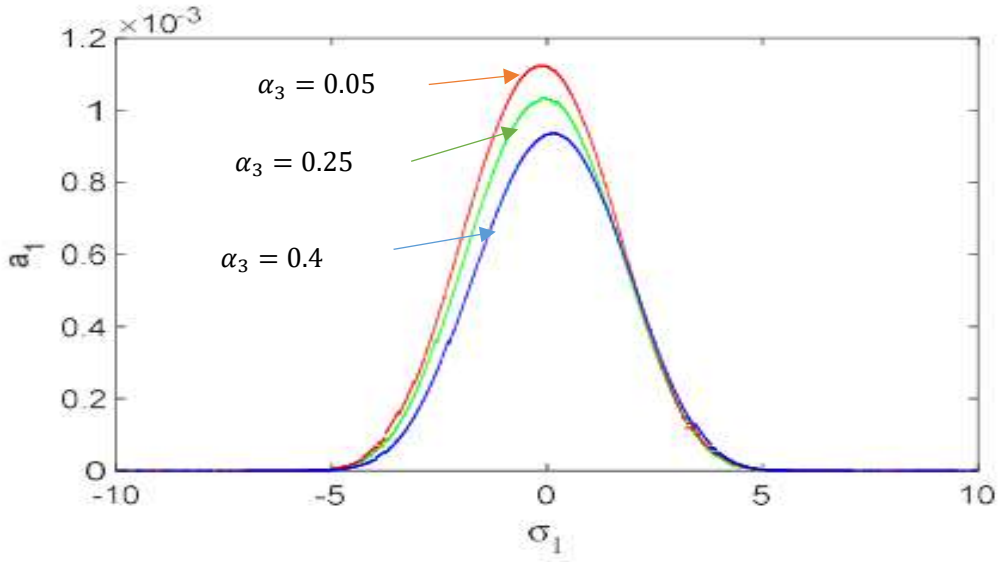

Figure 12. Influence of nonlinear control parameter α_3 (M.D).

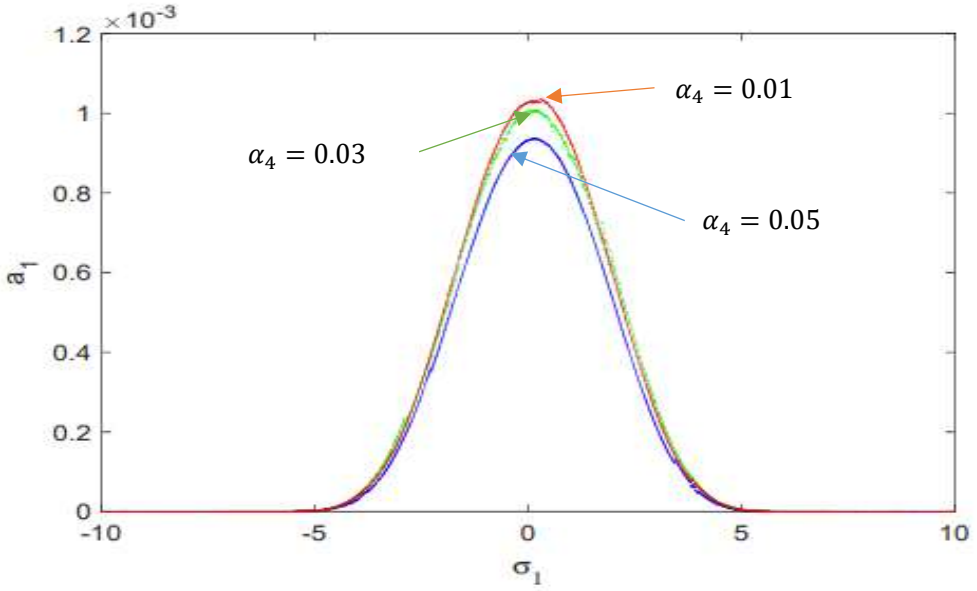

Figure 13. Influence of nonlinear control parameter α_4 (M.D).

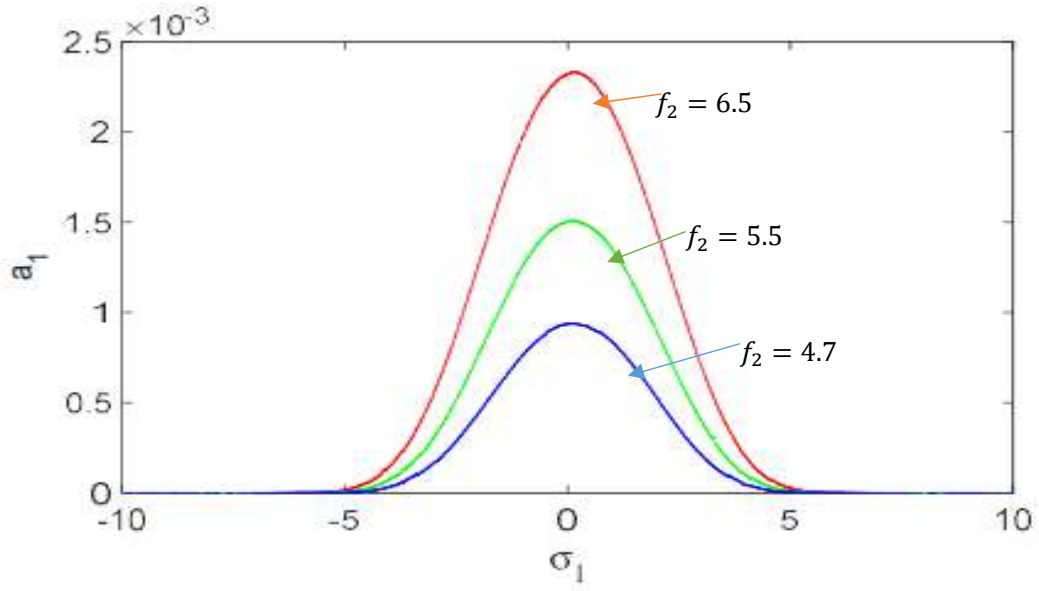

Figure 14. Influence of parametric excitation force parameter f_2 (M.I).

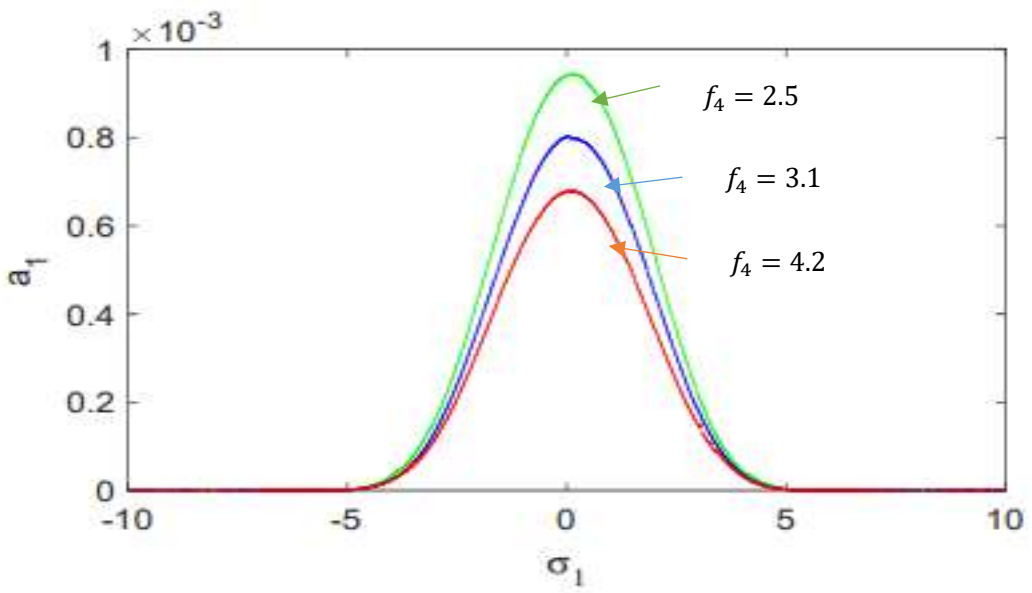

Figure 15. Influence of parametric excitation force parameter f_4 (M.D).

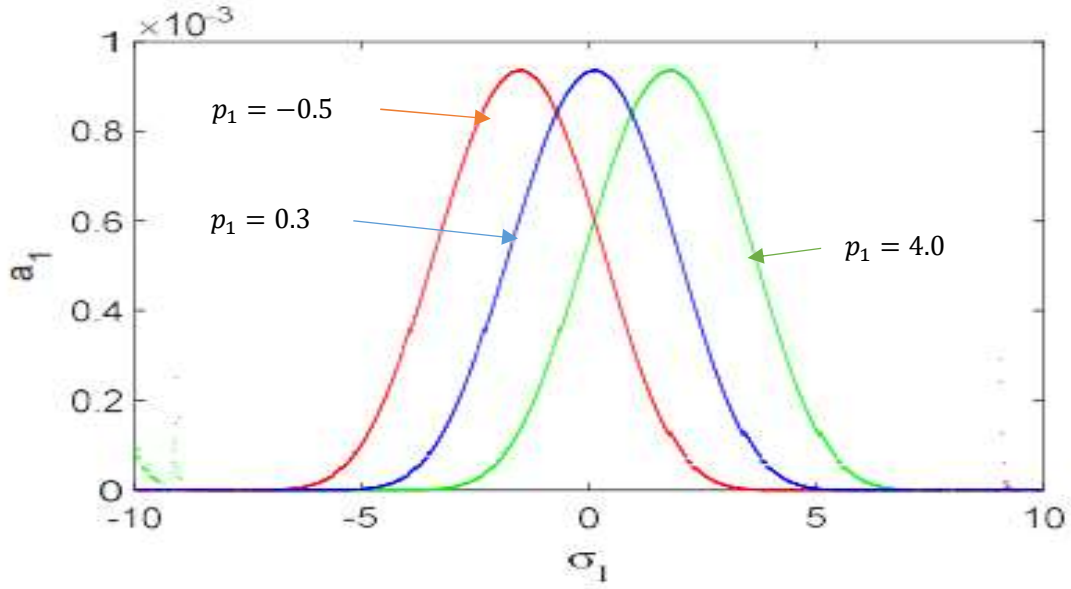

Figure 16. Influence of the linear control force coefficient p_1 at increasing amplitude moved to right, at decreasing amplitude moved to left.

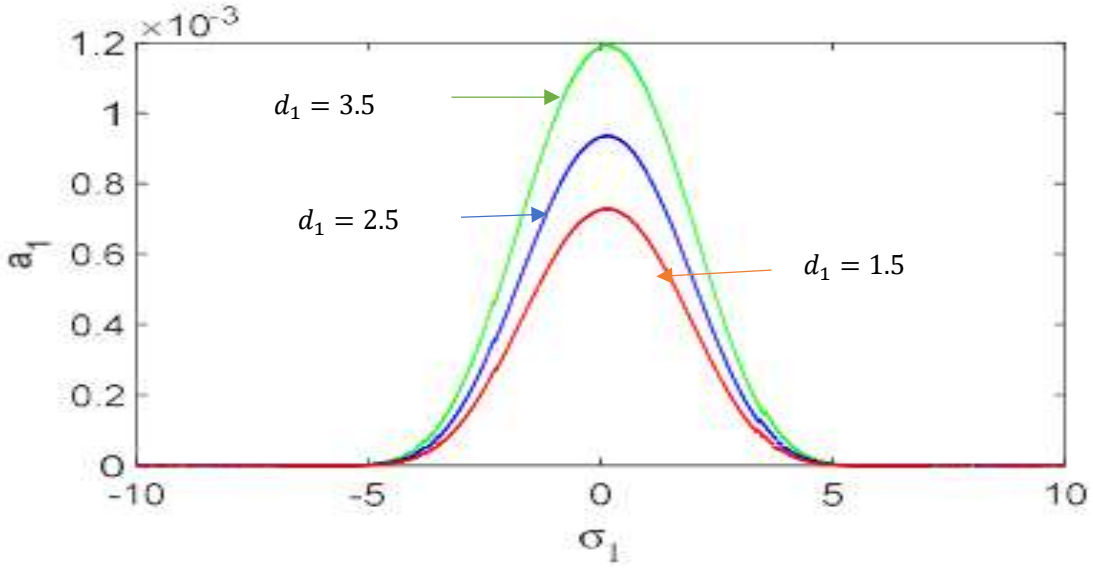

Figure 17. Influence of the linear control force coefficient d_1 (M.I).

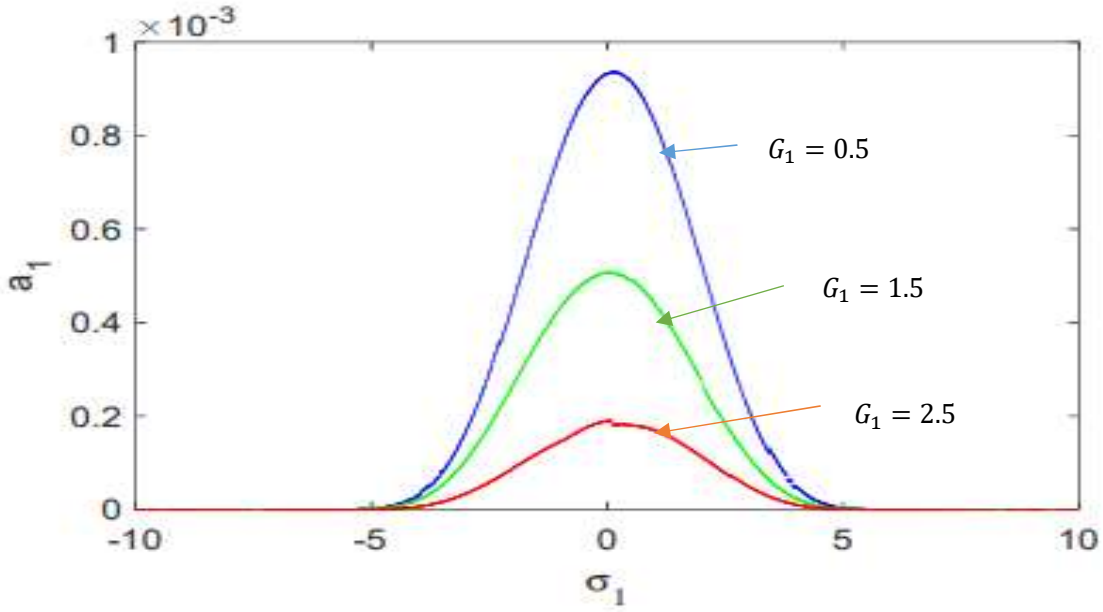

Figure 18. Influence of nonlinear control gain G_1 (M.D).

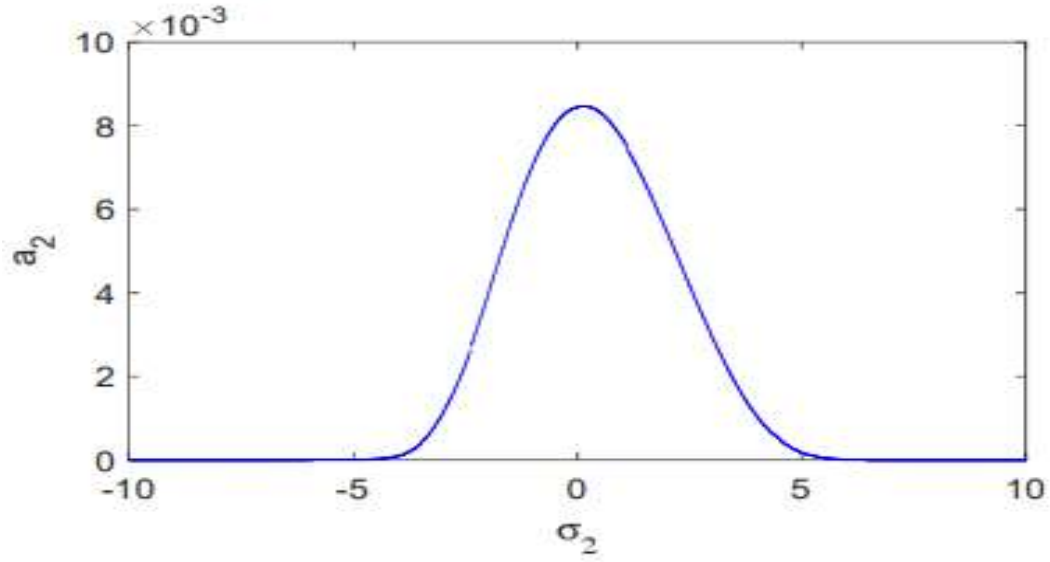

Figure 19. Influence response curves a_2 versus σ_2 of the controlled system.

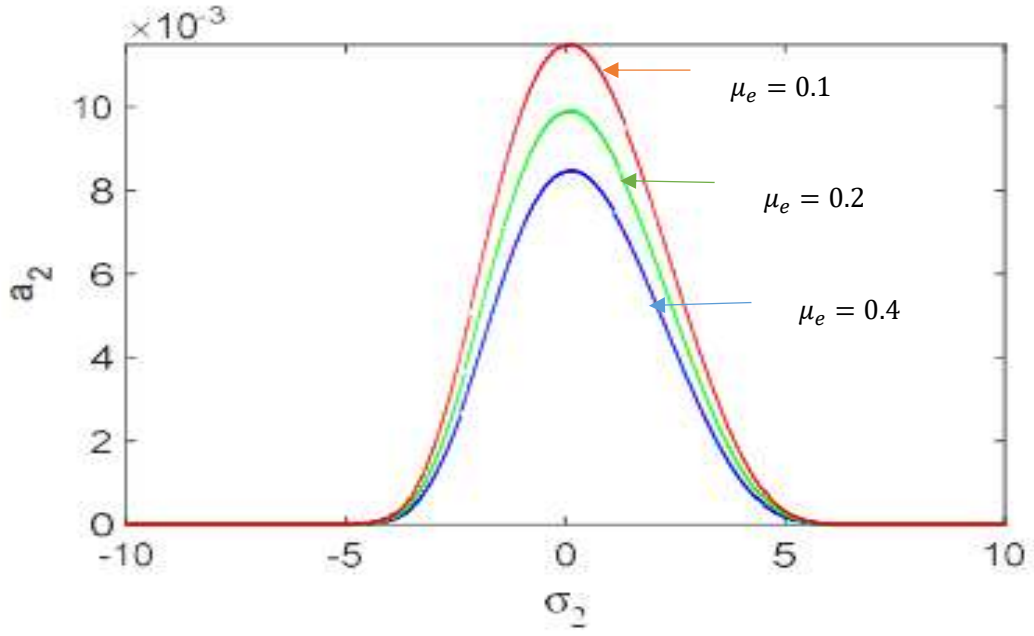

Figure 20. Impact of the damping coefficient μ_e (M.D).

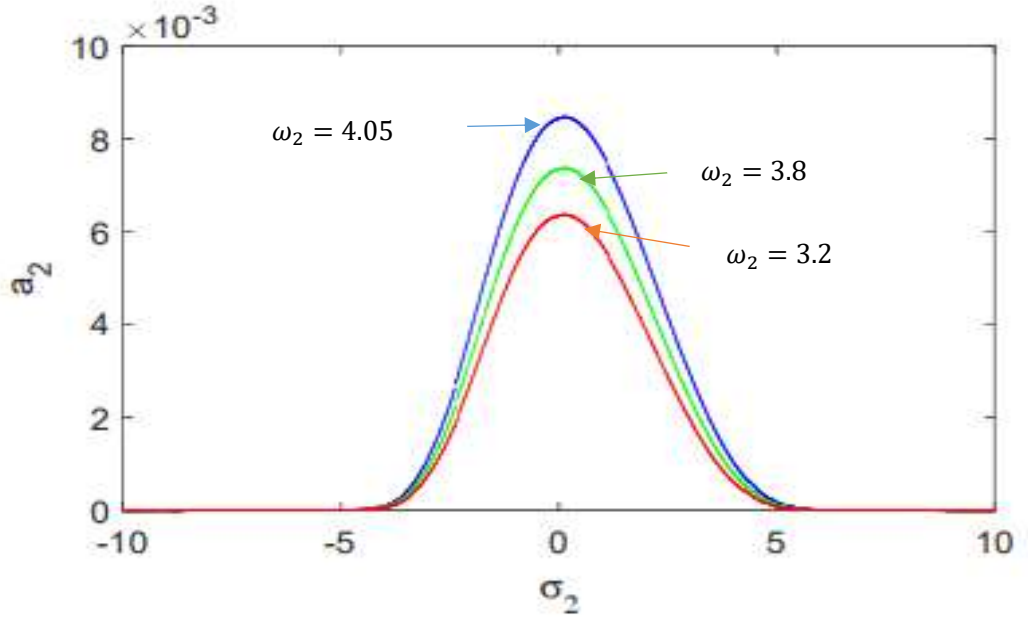

Figure 21. Effect of the excitation frequency ω_2 (M.I).

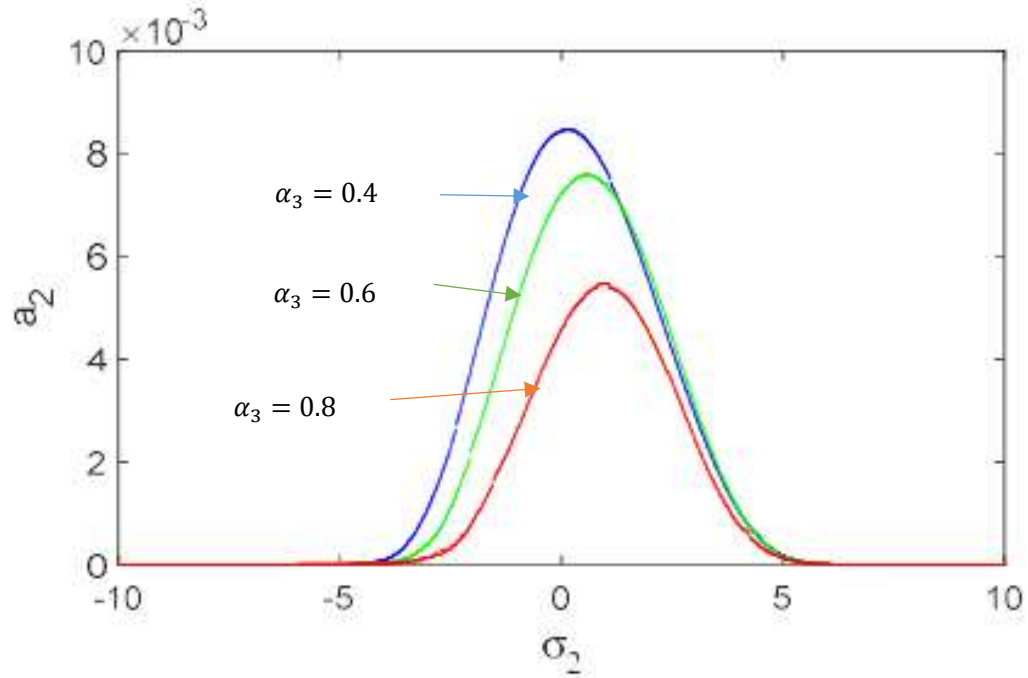

Figure 22. Influence of nonlinear control parameter α_3 (M.D).

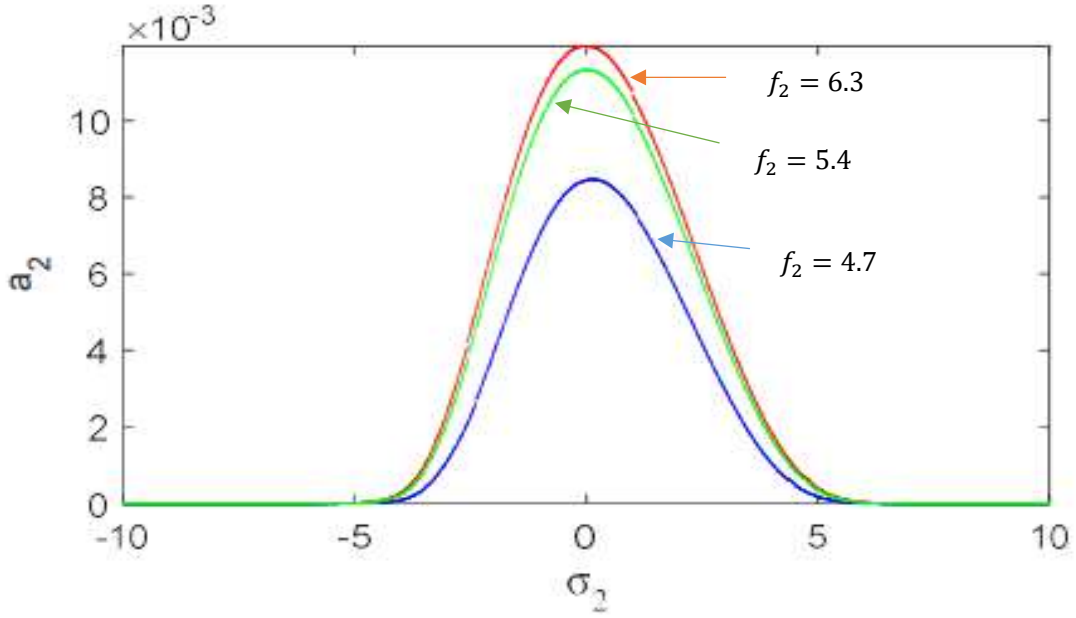

Figure 23. Influence of the parametric excitation force parameter f_2 (M.I).

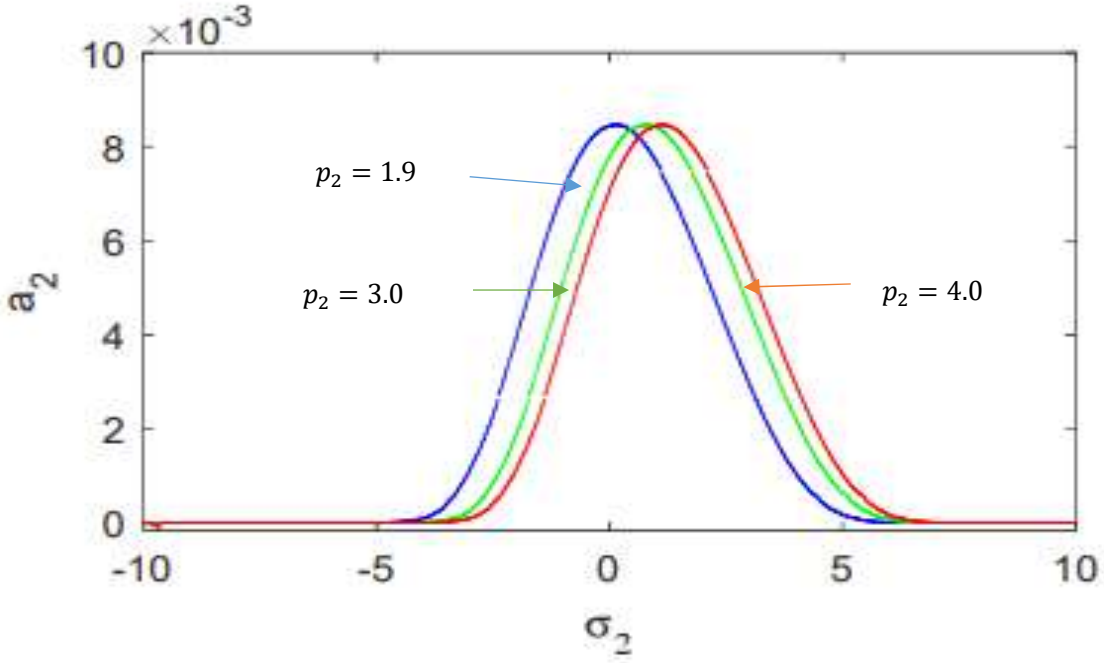

Figure 24. Influence of the linear control force factor p_2, at increasing amplitude it moved to right, but at decreasing amplitude it shifted to left.

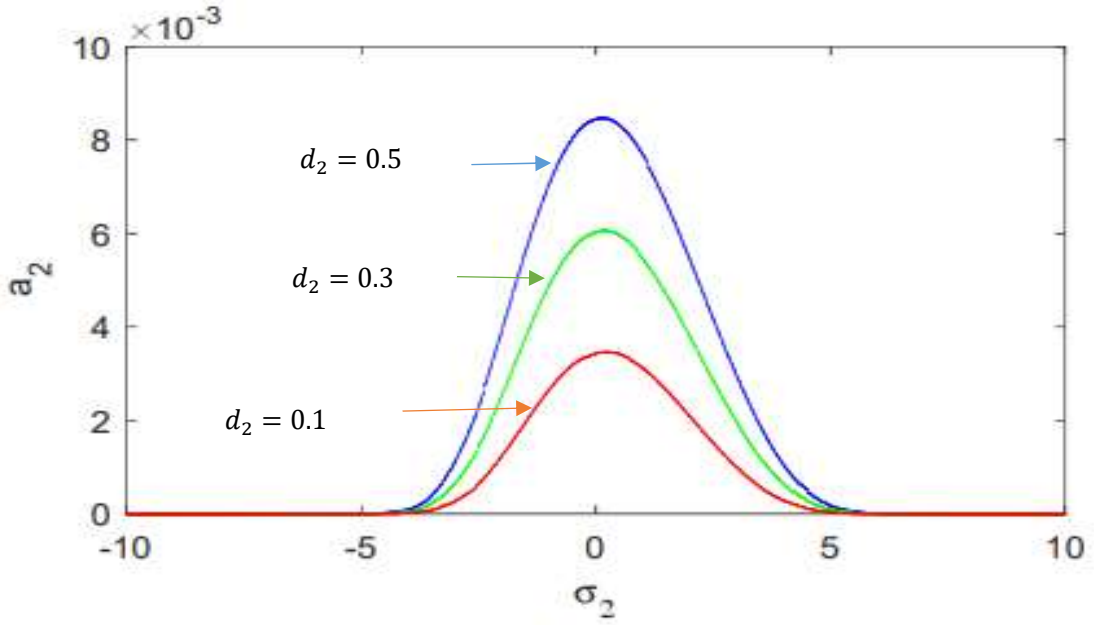

Figure 25. Influence of the linear control force coefficient d_2 (M.I).

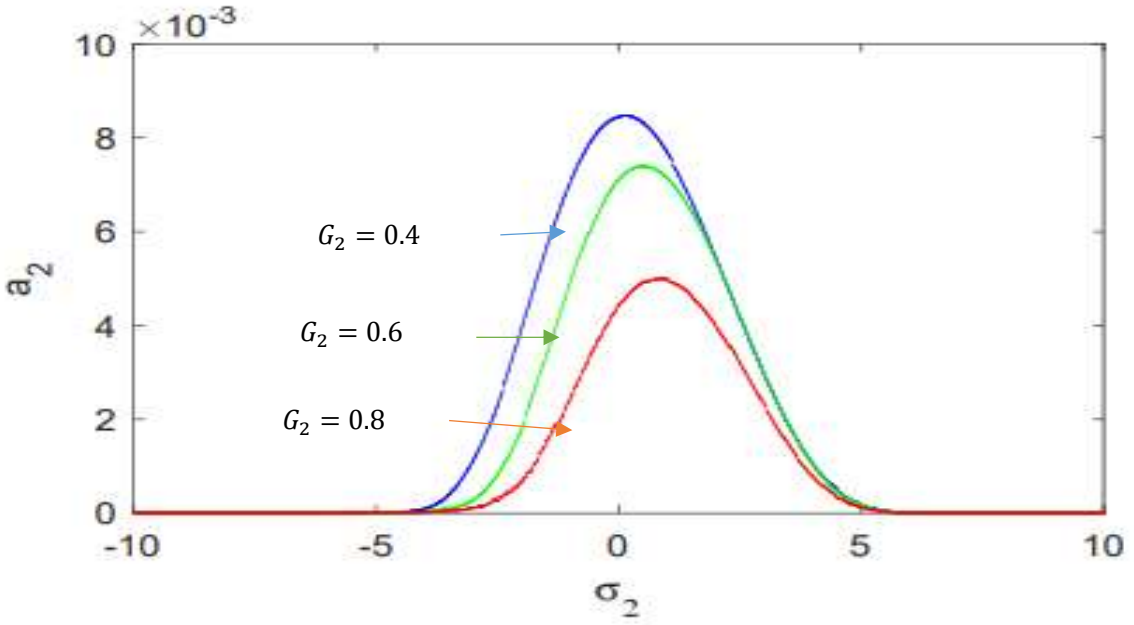

Figure 26. Influence of the nonlinear control gain G_2 (M.D).

Therefore, Table 2 provides a detailed account of the effects of various parameters of the controlled system with various effects on the system to appear the stable regions.

Table 2. Impact of various coefficients of the controlled system.

Parameter	Symbol	Status	Amplitude	Effect	Stability	Figure No.
Linear damping	μ_m	Increase	a_1	Decrease	Stable regions occur	8
Excitation frequency	ω_1	Increase	a_1	Increase	Stable regions occur	9
Excitation frequency	ω_2	Increase	a_1	Slightly Increase	Stable regions occur	10
Nonlinear control	α_2	Increase	a_1	Slightly Decrease	Stable regions occur	11
Nonlinear control	α_3	Increase	a_1	Decrease	Stable regions occur	12
Nonlinear control	α_4	Increase	a_1	Decrease	Stable regions occur	13
Parametric excitation force	f_2	Increase	a_1	Increase	Stable regions occur	14
parametric excitation force	f_4	Increase	a_1	Decrease	Stable regions occur	15
Linear control force	p_1	Increase	a_1	Shifted to right	Stable regions occur	16
		Decrease		Shifted to left		
Linear control force	d_1	Increase	a_1	Increase	Stable regions occur	17
Gain	G_1	Increase	a_1	Decrease	Stable regions occur	18
Linear damping	μ_e	Increase	a_2	Decrease	Stable regions occur	20
Excitation frequency	ω_2	Increase	a_2	Increase	Stable regions occur	21
Nonlinear control	α_3	Increase	a_2	Decrease	Stable regions occur	22
Parametric excitation force	f_2	Increase	a_2	Increase	Stable regions occur	23
Linear control force	p_2	Increase	a_2	Shifted to right	Stable regions occur	24
		Decrease		Shifted to left		
Linear control force	d_2	Increase	a_2	Increase	Stable regions occur	25
Gain	G_2	Increase	a_2	Decrease	Stable regions occur	26

5.3 Comparison of the same model with more recent studies

An electromechanical seismograph model associated electric circuit model system akin to Eq (2.7) was examined in [9–11]. However, they applied the multiple time scale process within the principal parametric resonance item to study the behaviour of the structure under mixed excitations, eliminating the need for a controller. The development of the model given in [11] is examined in the current work. I add a variety of control strategies to the vibrating structure system's modified system in order to determine which one reduces the framework structure's risk of vibration. Additionally, the upgraded system's new controller NPDVF is examined in this article. The results of this research show that the novel controller less than the other controllers decreases the high vibrational amplitude of the model exposed to parametric stimulation inside the simultaneous resonance, as shown in subsection 5.1. The perturbation approach is used to aid in the acquisition of analytical solutions. Plotting of the frequency response graphs occurs at different framework parameter levels. We end with a numerical validation of the obtained results. The comparisons show that the current approach produces findings that are remarkably similar to those found in [11] and that the discrepancies are less than 1%.

5.4 Comparison between the proposed NPDVF control and other nonlinear controllers of nonlinear systems

A comparison between nonlinear controllers with the proposed NPDVF controller is presented in a summary Table 3 that compares the performance of the different controllers based on the criteria of robustness, computational cost, and control signal amplitude. The table should provide a clear visual comparison that illustrates the advantages of the proposed NPDVF controller.

Table 3. Comparison NPDVF controller with other controllers of nonlinear systems.

Control Method	Robustness	Computational Cost	Control Signal Amplitude
NPDVF Controller	Excellent (handles nonlinearities and bifurcations)	Low (efficient and fast)	Small (efficient suppression)
Linear Proportional-Derivative (PD) Controller	Moderate (struggles with nonlinearities)	Very Low (simple)	Large (less adaptive)
Sliding Mode Controller (SMC)	High (robust but chattering)	Moderate (requires switching)	Large (due to chattering)
Fuzzy Logic Controller	Moderate (requires rule tuning)	Moderate (rule evaluation)	Moderate (tuned control)
Model Predictive Controller (MPC)	High (optimal performance but computationally expensive)	Very High (optimization)	Moderate to Large (depends on prediction)
Backstepping Controller	High (effective for nonlinear systems)	Moderate (recursive equations)	Moderate to Large (strong control action)

5.5 Disturbance unavoidably of main control coefficients of the proposed controlled model

The time response of control inputs is shown in Figures 27–32 where the control input is also used to eliminate the effect of disturbance mainly at the stable stage. The control inputs is not only regulating the system's behavior but is also designed to mitigate the effect of external disturbances, particularly during the stable stage of the system's operation. These figures will show how the control input varies over time as the system responds to a disturbance. Each figure shows how the control input changes over time and responds to disturbances, providing a clear visualization of the controller's effectiveness in rejecting disturbances. This suggests that the system can quickly react to external disturbances, with the linear control force $p_1 = 2.3$ stabilizing at a specific value after some initial disturbance. The system reaches stability within a short time, indicating a fast disturbance rejection process, and the disturbance effect is effectively mitigated as in Figure 27. Also, Figure 28 shows that the system achieves a disturbance-free state after a brief period. The disturbance input $d_1 = 2.5$ has been neutralized quickly, indicating that the controller effectively nullifies the impact of the disturbance on the system in a short time. The nonlinear control gain $G_1 = 0.5$ is an important factor in reducing disturbances. When this gain is set to 0.5, it appears that the system is better able to suppress disturbances. This indicates that the nonlinear controller is tuned to counteract the disturbances effectively, ensuring that the system can reach a steady state despite the presence of external influences as in Figure 29. Additionally, the control parameters p_2 and d_2 appear to be carefully selected to ensure the system reacts appropriately to disturbances while maintaining stability. The values of $p_2 = 1.9$ and $d_2 = 0.5$ are likely optimized for quick disturbance rejection and minimal control effort. These parameters ensure that the system reaches the desired state quickly, further reducing the influence of external disturbances as shown in Figures 30 and 31. Finally, When $G_1 = 0.4$ is applied, the system is better able to reduce or even eliminate the impact of external disturbances. The system's response, particularly in terms of the control input, should show a clear improvement after this nonlinear gain is activated, resulting in a smoother and more stable control input over time as illustrated in Figure 32. By effectively control input parameters such as $p_1, p_2, d_1, d_2, G_{1,}$ and G_2, the system is able to reject disturbances in a timely manner and ensure robust performance.

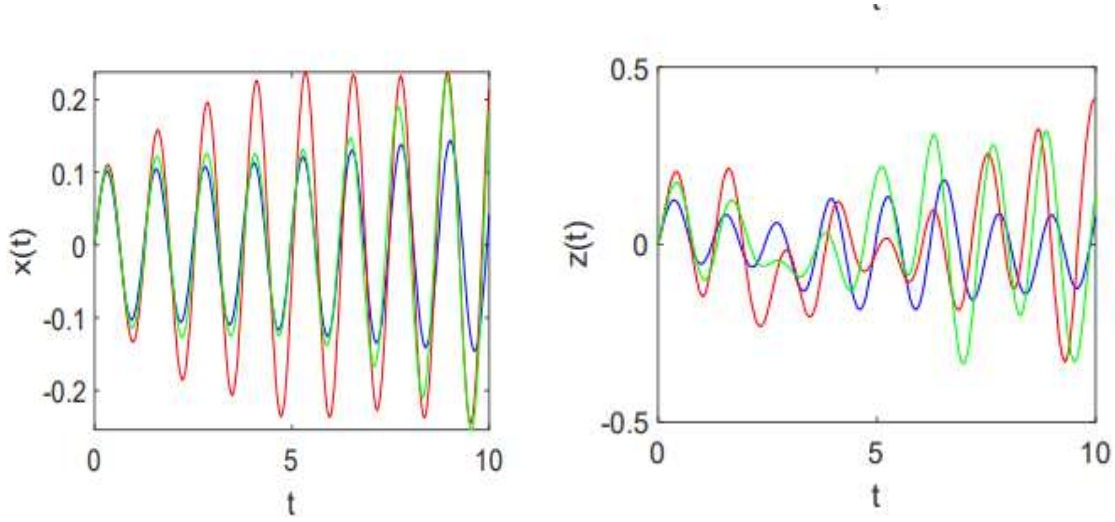

Figure 27. Time response of linear control force p_1 (—— 2.3, —— 3.5, —— 5.5).

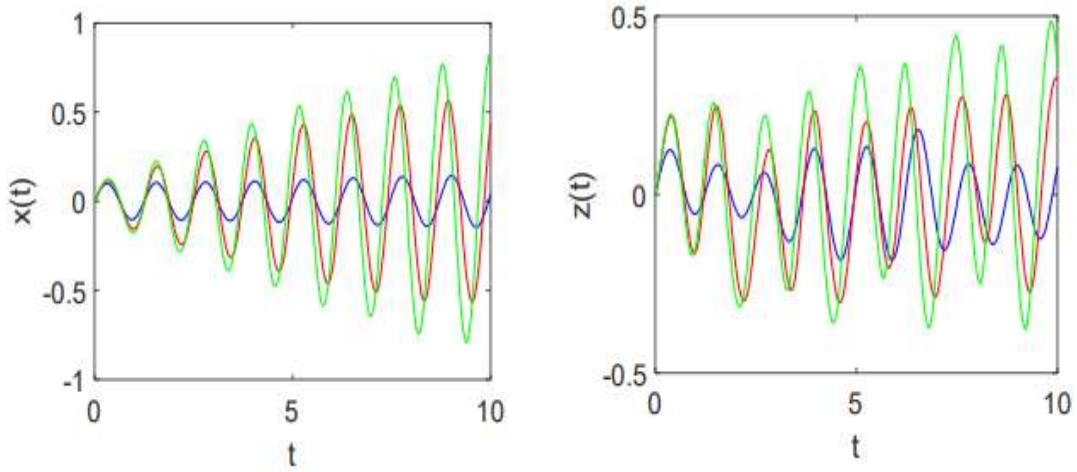

Figure 28. Time response of linear control force d_1 (—— 2.5, —— 4.5, —— 6.5).

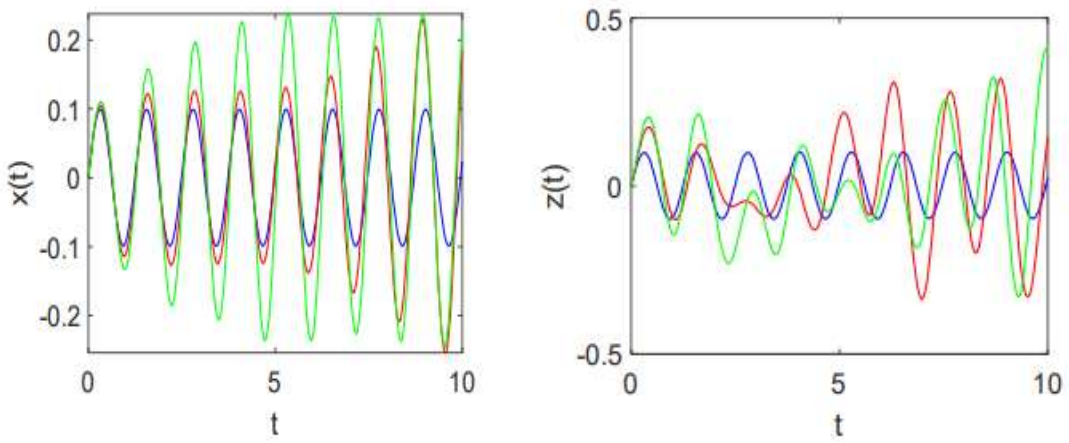

Figure 29. Time response of nonlinear control gain G_1 (—— 0.5, —— 1.5, —— 3.5).

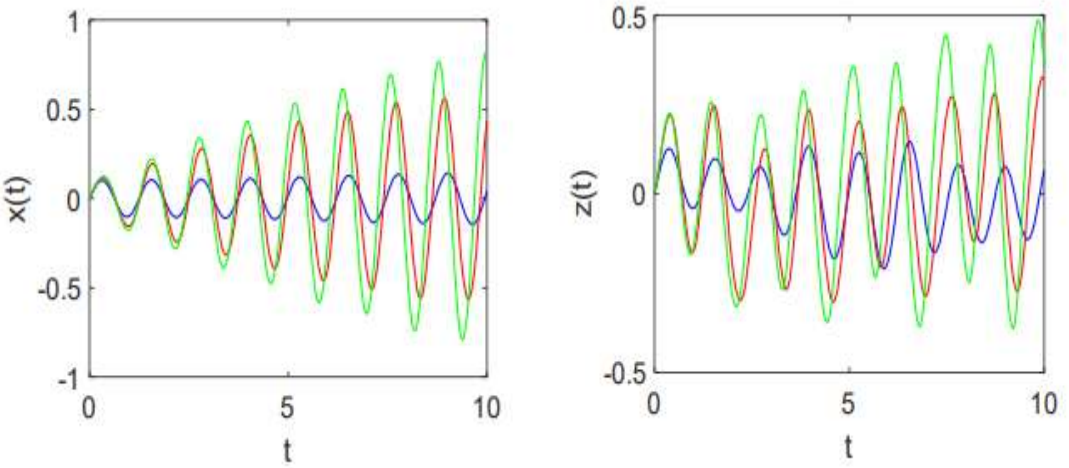

Figure 30. Time response of linear control force p_2 (—— 1.9, —— 3.2, —— 4.4).

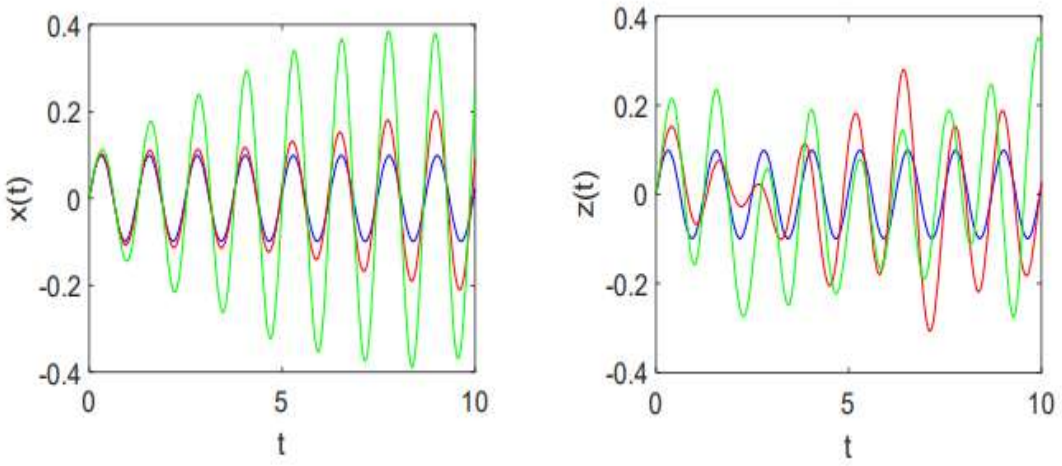

Figure 31. Time response of linear control force d_2 (—— 0.5, —— 1.5, —— 3.5).

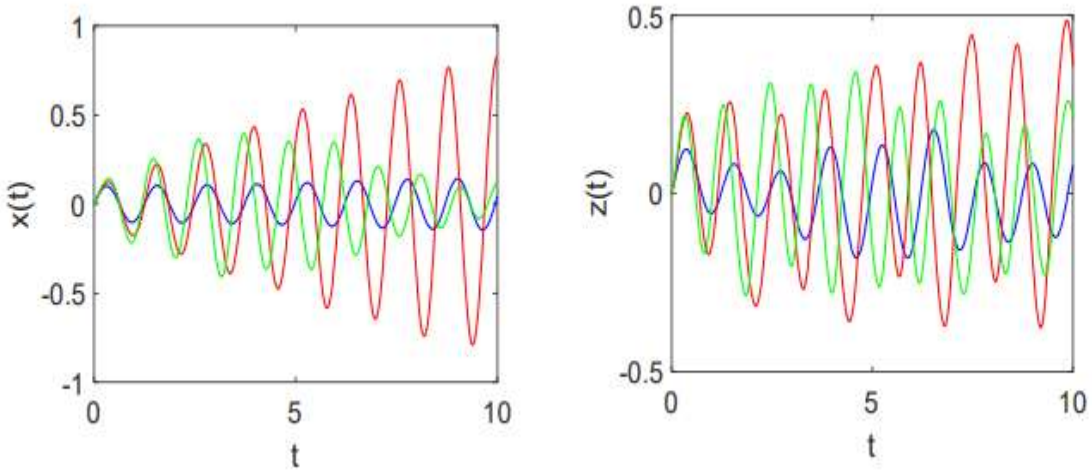

Figure 32. Time response of nonlinear control gain G_2 (—— 0.4, —— 3.3, —— 1.5).

6. Conclusions

This study introduces a novel nonlinear proportional-derivative cubic velocity feedback (NPDVF) Controller that effectively manages vibrations in systems with coupled mechanical and electrical components. The controller's performance has been validated through numerical simulations and perturbation methods, demonstrating its ability to reduce vibrations, stabilize nonlinear motions, and suppress unwanted oscillations in the presence of mixed forces. A number of controller design approaches (PD control, NCVF control, and NPDVF as an innovative control method) were assessed in order to ascertain which one best minimizes high amplitude vibrations during the simultaneous resonance case $\Omega_2 \cong \omega_1, \Omega_4 \cong \omega_2$. The solution of the studied controlled model can be approximated using the perturbation approach. The key advantages of the NPDVF controller, including its robustness to parameter uncertainties and external disturbances, low computational cost, and efficient control

signal amplitude, make it a promising solution for nonlinear vibration control systems. A comprehensive comparison with traditional control strategies, such as PD control**,** sliding mode control (SMC), and model predictive control (MPC), highlights the superior performance of the NPDVF controller in several aspects. Specifically, the NPDVF controller outperforms others in terms of computational efficiency and robustness, while also maintaining a smaller control signal amplitude, which reduces actuator wear and improves energy efficiency. These results suggest that the NPDVF controller is an effective and practical solution for real-time vibration control in complex systems. This study advances our understanding of the control dynamics in nonlinear models with combined excitations via perturbation technique for controlling chaotic behavior in such models. Future work could investigate the impact of time delay on the effectiveness of the NPDVF controller. Specifically, it would be beneficial to analyze how time delay influences the system's stability, vibration reduction, and bifurcation control.

Use of Generative-AI tools declaration

The author declares he has not used Artificial Intelligence (AI) tools in the creation of this article.

Acknowledgments

The author extends his appreciation to Prince Sattam bin Abdulaziz University for funding this research work through the project number (PSAU/ 2024/01/29249).

Conflict of interest

The author declares that he has no known competing financial interests or personal relationships that could have appeared to influence the work reported in this paper.

References

1. R. Yamapi, J. B. C. Orou, P. Woafo, Harmonic oscillations, stability and chaos control in a nonlinear electromechanical system, *J. Sound Vib.*, **259** (2003), 1253–1264. https://doi.org/10.1006/jsvi.2002.5289
2. Z. M. Ge, T. N. Lin, Chaos, Chaos control and synchronization of electro-mechanical gyrostat system, *J. Sound Vib.*, **259** (2003), 585–603. https://doi.org/10.1006/jsvi.2002.5110
3. R. Yamapi, S. Bowong, Dynamics and chaos control of the self-sustained electromechanical device with and without discontinuity, *Commun. Nonlinear Sci.*, **11** (2006), 355–375. https://doi.org/10.1016/j.cnsns.2004.09.002
4. M. Siewe Siewe, F. M. M. Kakmeni, S. Bowong, C. Tchawoua, Non-linear response of a self-sustained electromechanical seismographs to fifth resonance excitations and chaos control, *Chaos Soliton. Fract.*, **29** (2006), 431–445. https://doi.org/10.1016/j.chaos.2005.08.210
5. R. Yamapi, F. M. M. Kakmeni, J. B. C. Orou, Nonlinear dynamics and synchronization of coupled electromechanical systems with multiple functions, *Commun. Nonlinear Sci.*, **12** (2007), 543–567. https://doi.org/10.1016/j.cnsns.2005.05.003

6. R. Yamapi, M. A. Aziz-Alaoui, Vibration analysis and bifurcations in the self-sustained electromechanical system with multiple functions, *Commun. Nonlinear Sci.*, **12** (2007), 1534–1549. https://doi.org/10.1016/j.cnsns.2006.03.001
7. C. A. K. Kwuimy, P. Woafo, Dynamics of a self-sustained electromechanical system with flexible arm and cubic coupling, *Commun. Nonlinear Sci.*, **12** (2007), 1504–1517. https://doi.org/10.1016/j.cnsns.2006.03.003
8. C. A. K. Kwuimy, P. Woafo, Dynamics, chaos and synchronization of self-sustained electromechanical systems with clamped-free flexible arm, *Nonlinear Dyn.*, **53** (2008), 201–213. https://doi.org/10.1007/s11071-007-9308-0
9. G. S. M. Ngueuteu, R. Yamapi, P. Woafo, Effects of higher nonlinearity on the dynamics and synchronization of two coupled electromechanical devices, *Commun. Nonlinear Sci.*, **13** (2008), 1213–1240. https://doi.org/10.1016/j.cnsns.2006.09.013
10. U. H. Hegazy, Dynamics and control of a self-sustained electromechanical seismograph with time varying stiffness, *Meccanica*, **44** (2009), 355–368. https://doi.org/10.1007/s11012-008-9171-1
11. M. S. Siewe, W. F. Kenfack, T. C. Kofane, Probabilistic response of an electromagnetic transducer with nonlinear magnetic coupling under bounded noise excitation, *Chaos Soliton. Fract.*, **124** (2019), 26–35. https://doi.org/10.1016/j.chaos.2019.04.030
12. Y. A. Amer, Resonance and vibration control of two-degree-of-freedom nonlinear electromechanical system with harmonic excitation, *Nonlinear Dyn.*, **81** (2015), 2003–2019. https://doi.org/10.1007/s11071-015-2121-2
13. Y. A. Amer, H. S. Bauomy, M. Sayed, Vibration suppression in a twin-tail system to parametric and external excitations, *Comput. Math. Appl.*, **58** (2009), 1947–1964. https://doi.org/10.1016/j.camwa.2009.07.090
14. M. Sayed, A. A. Mousa, Second-order approximation of angle-ply composite laminated thin plate under combined excitations, *Commun. Nonlinear Sci.*, **17** (2012), 5201–5216. https://doi.org/10.1016/j.cnsns.2012.04.003
15. M. Sayed, A. A. Mousa, Vibration, stability, and resonance of angle-ply composite laminated rectangular thin plate under multi-excitations, *Math. Probl. Eng.*, **2013** (2013), 418374. https://doi.org/10.1155/2013/418374
16. A. A. Mousa, M. Sayed, I. M. Eldesoky, W. Zhang, Nonlinear stability analysis of a composite laminated piezoelectric rectangular plate with multi-parametric and external excitations, *Int. J. Dynam. Control*, **2** (2014), 494–508. https://doi.org/10.1007/s40435-014-0057-x
17. M. Sayed, A. A. Mousa, I. H. Mustafa, Stability analysis of a composite laminated piezoelectric plate subjected to combined excitations, *Nonlinear Dyn.*, **86** (2016), 1359–1379. https://doi.org/10.1007/s11071-016-2969-9
18. Y. S. Hamed, Y. A. Amer, Nonlinear saturation controller for vibration supersession of a nonlinear composite beam, *J. Mech. Sci. Technol.*, **28** (2014), 2987–3002. https://doi.org/10.1007/s12206-014-0706-1
19. Y. S. Hamed, A.T. El-Sayed, E. R. El-Zahar, On controlling the vibrations and energy transfer in MEMS gyroscopes system with simultaneous resonance, *Nonlinear Dyn.*, **83** (2016), 1687–1704. https://doi.org/10.1007/s11071-015-2440-3
20. M. P. Cartmell, *Introduction to linear, parametric and nonlinear vibrations*, London: Chapman and Hall, 1990.

21. A. H. Nayfeh, B. Balachandran, *Applied nonlinear dynamics: Analytical, computational and experimental methods*, New York: Wiley, 1995. https://doi.org/10.1002/9783527617548
22. E. V. Pankratova, V. N. Belykh, Consequential noise-induced synchronization of indirectly coupled self-sustained oscillators, *Eur. Phys. J. Spec. Top.*, **222** (2013), 2509–2515. https://doi.org/10.1140/epjst/e2013-02033-8
23. V. N. Belykh, E. V. Pankratova, Chaotic dynamics of two van der pol-duffing oscillators with huygens coupling, *Regul. Chaot. Dyn.*, **15** (2010), 274–284. https://doi.org/10.1134/S1560354710020140
24. W. Martens, U. Von Wagner, G. Litak, Stationary response of nonlinear magneto-piezoelectric energy harvester systems under stochastic excitation, *Eur. Phys. J. Spec. Top.*, **222** (2013), 1665–1673. https://doi.org/10.1140/epjst/e2013-01953-5
25. M. Borowiec, G. Litak, S. Lenci, Noise effected energy harvesting in a beam with stopper, *Int. J. Struct. Stab. Dy.*, **14** (2014), 1440020. https://doi.org/10.1142/S0219455414400203
26. M. Xu, X. Jin, Y. Wang, Z. Huang, Stochastic averaging for nonlinear vibration energy harvesting system, *Nonlinear Dyn.*, **78** (2014),1451–1459. https://doi.org/10.1007/s11071-014-1527-6
27. H. Li, W. Qin, C. Lan, W. Deng, Z. Zhou, Dynamics and coherence resonance of tri-stable energy harvesting system, *Smart Mater. Struct.*, **25** (2016), 015001. https://doi.org/10.1088/0964-1726/25/1/015001
28. K. M. Harish, B. J. Gallacher, J. S. Burdess, J. A. Neasham, Experimental investigation of parametric and externally forced motion in resonant MEMS sensors, *J. Micromech. Microeng.*, **19** (2008), 015021. https://doi.org/10.1088/0960-1317/19/1/015021
29. L. A. Oropeza-Ramos, C. B. Burgner, K. L. Turner, Robust micro-rate sensor actuated by parametric resonance, *Sensor. Actuat. A phys.*, **152** (2009), 80–87. https://doi.org/10.1016/j.sna.2009.03.010
30. M. Pallay, M. Daeichin, S. Towfighian, Feasibility study of a MEMS threshold-pressure sensor based on parametric resonance: experimental and theoretical investigations, *J. Micromech. Microeng.*, **31** (2021), 025002. https://doi.org/10.1088/1361-6439/abce9c
31. W. Zhang, R. Baskaran, K. L. Turner, Effect of cubic nonlinearity on auto-parametrically amplified resonant MEMS mass sensor, *Sensor. Actuat. A phys.*, **102** (2002), 139–150. https://doi.org/10.1016/S0924-4247(02)00299-6
32. X. Y. Mao, H. Ding, L. Q. Chen, Parametric resonance of a translating beam with pulsating axial speed in the supercritical regime, *Mech. Res. Commun.*, **76** (2016), 72–77. https://doi.org/10.1016/j.mechrescom.2016.07.008
33. J. F. Rhoads, S. W. Shaw, K. L. Foster, J. Moehlis, Generalized parametric resonance in electrostatically actuated microelectromechanical oscillators, *J. Sound Vib.*, **296** (2006), 797–829. https://doi.org/10.1016/j.jsv.2006.03.009
34. J. F. Rhoads, S. W. Shaw, K. L. Turner, The nonlinear response of resonant microbeam systems with purely parametric electrostatic actuation, *J. Micromech. Microeng.*, **16** (2006), 890–899. https://doi.org/10.1088/0960-1317/16/5/003
35. M. S. Siewe, C. Tchawoua, S. Rajasekar, Parametric resonance in the Rayleigh-Duffing oscillator with time-delayed feedback, *Commun. Nonlinear Sci.*, **17** (2012), 4485–4493. https://doi.org/10.1016/j.cnsns.2012.02.030

36. M. Aghamohammadi, V. Sorokin, B. Mace, On the response attainable in nonlinear parametrically excited systems, *Appl. Phys. Lett.*, **115** (2019), 154102. https://doi.org/10.1063/1.5120434
37. S. Chen, B. Epureanu, Forecasting bifurcations in parametrically excited systems, *Nonlinear Dyn.*, **91** (2018), 443–457. https://doi.org/10.1007/s11071-017-3880-8
38. J. Warminski, Nonlinear dynamics of self-, parametric, and externally excited oscillator with time delay: van der Pol versus Rayleigh models, *Nonlinear Dyn.*, **99** (2020), 35–56. https://doi.org/10.1007/s11071-019-05076-5
39. J. Warminski, Frequency locking in a nonlinear MEMS oscillator driven by harmonic force and time delay, *Int. J. Dynam. Control*, **3** (2015), 122–136. https://doi.org/10.1007/s40435-015-0152-7
40. D. Li, S. W. Shaw, The effects of nonlinear damping on degenerate parametric amplification, *Nonlinear Dyn.*, **102** (2020), 2433–2452. https://doi.org/10.1007/s11071-020-06090-8
41. S. Zaitsev, O. Shtemppluck, E. Buks, O. Gottlieb, Nonlinear damping in a micromechanical oscillator, *Nonlinear Dyn.*, **67** (2012), 859–883. https://doi.org/10.1007/s11071-011-0031-5
42. S. Gutschmidt, O. Gottlieb, Nonlinear dynamic behavior of a microbeam array subject to parametric actuation at low, medium and large DC-voltages, *Nonlinear Dyn.*, **67** (2012), 1–36. https://doi.org/10.1007/s11071-010-9888-y
43. A. H. Nayfeh, D. Mook, *Nonlinear oscillations*, New York: Wiley, 1995. https://doi.org/10.1002/9783527617586
44. A. T. El-Sayed, H. S. Bauomy, Outcome of special vibration controller techniques linked to a cracked beam, *Appl. Math. Model.*, **63** (2018), 266–287. https://doi.org/10.1016/j.apm.2018.06.045
45. A. T. El-Sayed, H. S. Bauomy, A beam-ring circular truss antenna restrained by means of the negative speed feedback procedure, *J. Vib. Control*, **28** (2022), 2032–2051. https://doi.org/10.1177/10775463211003698
46. A. T. El-Sayed, H. S. Bauomy, NIPPF versus ANIPPF controller outcomes on semi-direct drive cutting transmission system in a shearer, *Chaos Soliton. Fract.*, **156** (2022), 111778. https://doi.org/10.1016/j.chaos.2021.111778
47. H. S. Bauomy, A. T. El-Sayed, Vibration performance of a vertical conveyor system under two simultaneous resonances, *Arch. Appl. Mech.*, **88** (2018), 1349–1368. https://doi.org/10.1007/s00419-018-1375-9
48. H. S. Bauomy, A. T. El-Sayed, A new six-degrees of freedom model designed for a composite plate through PPF controllers, *Appl. Math. Model.*, **88** (2020), 604–630. https://doi.org/10.1016/j.apm.2020.06.067
49. H. S. Bauomy, A. T. El-Sayed, Act of nonlinear proportional derivative controller for MFC laminated shell, *Phys. Scr.*, **95** (2020), 095210. https://doi.org/10.1088/1402-4896/abaa7c
50. H. S. Bauomy, A. T. El-Sayed, Mixed controller (IRC+NSC) involved in the harmonic vibration response cantilever beam model, *Meas. Control*, **53** (2020), 1954–1967. https://doi.org/10.1177/0020294020964243
51. H. S. Bauomy, A. T. El-Sayed, Nonlinear saturation controller simulation for reducing the high vibrations of a dynamical system, *Math. Biosci. Eng.*, **19** (2022), 3487–3508. https://doi.org/10.3934/mbe.2022161
52. H. S. Bauomy, New controller (NPDCVF) outcome of FG cylindrical shell structure, *Alex. Eng. J.*, **61** (2022), 1779–1801. https://doi.org/10.1016/j.aej.2021.06.061

53. A. H. Nayfeh, *Perturbation methods*, New York: Wiley, 2000. https://doi.org/10.1002/9783527617609
54. X. Q. Fang, Q. L. He, H. W. Ma, C. S. Zhu, Multi-field coupling and free vibration of a sandwiched functionally-graded piezoelectric semiconductor plate, *Appl. Math. Mech.,* **44** (2023), 1351–1366. https://doi.org/10.1007/s10483-023-3017-6
55. X. Q. Fang, H. W. Ma, C. S. Zhu, Non-local multi-fields coupling response of a piezoelectric semiconductor nanofiber under shear force, *Mech. Adv. Mater. Struc.*, **31** (2024), 2452–2459. https://doi.org/10.1080/15376494.2022.2158503
56. C. Liu, X. Yue, J. Zhang, K. Shi, Active disturbance rejection control for delayed Electromagnetic docking of spacecraft in elliptical orbits, *IEEE T. Aero. Elec. Sys.*, **58** (2022), 2257–2268. https://doi.org/10.1109/TAES.2021.3130830
57. B. Lyu, C. Liu, X. Yue, Integrated predictor-observer feedback control for vibration mitigation of large-scale spacecraft with unbounded input time delay, *IEEE T. Aero. Elec. Sys.*, **99** (2024), 1–12. https://doi.org/10.1109/TAES.2024.3505851
58. E. L. Rees, Graphical discussion of the roots of a quartic equation, *Am. Math. Mon.*, **29** (1922), 51–55. https://doi.org/10.2307/2972804
59. D. Lazard, Quantifier elimination: optimal solution for two classical examples, *J. Symb. Comput.*, **5** (1988), 261–266. https://doi.org/10.1016/S0747-7171(88)80015-4

AIMS Press